The 2dF Galaxy Redshift Survey: the population of nearby radio galaxies at the 1-mJy level

Manuela Magliocchetti,[1][*] Steve J. Maddox,[2] Carole A. Jackson,[3] Joss Bland-Hawthorn,[4] Terry Bridges,[4] Russell Cannon,[4] Shaun Cole,[5] Matthew Colless,[3] Chris Collins,[6] Warrick Couch,[7] Gavin Dalton,[9] Roberto de Propris,[7] Simon P. Driver,[8] George Efstathiou,[10] Richard S. Ellis,[11] Carlos S. Frenk,[4] Karl Glazebrook,[12] Ofer Lahav,[10] Ian Lewis,[4] Stuart Lumsden,[13] John A. Peacock,[14] Bruce A. Peterson,[3] Will Sutherland[14] and Keith Taylor[3]

[1]*SISSA, Via Beirut 4, 34100, Trieste, Italy*
[2]*School of Physics and Astronomy, University of Nottingham, Nottingham NG7 2RD*
[3]*Research School of Astronomy and Astrophysics, The Australian National University, Canberra, ACT 2611, Australia*
[4]*Anglo-Australian Observatory, PO Box 296, Epping, NSW 2121, Australia*
[5]*Department of Physics, University of Durham, South Road, Durham DH1 3LE*
[6]*Astrophysics Research Institute, Liverpool John Moores University, Twelve Quays House, Birkenhead L14 1LD*
[7]*Department of Astrophysics, University of New South Wales, Sydney, NSW 2052, Australia*
[8]*School of Physics and Astronomy, University of St Andrews, North Haugh, St Andrews, Fife KY6 9SS*
[9]*Department of Physics, University of Oxford, Keble Road, Oxford OX1 3RH*
[10]*Institute of Astronomy, University of Cambridge, Madingley Road, Cambridge CB3 0HA*
[11]*Department of Astronomy, California Institute of Technology, Pasadena, CA 91125, USA*
[12]*Department of Physics and Astronomy, Johns Hopkins University, Baltimore, MD 21218-2686, USA*
[13]*Department of Physics, University of Leeds, Woodhouse Lane, Leeds LS2 9JT*
[14]*Institute for Astronomy, University of Edinburgh, Royal Observatory, Blackford Hill, Edinburgh EH9 3HJ*

ABSTRACT

We use redshift determinations and spectral analysis of galaxies in the 2dF Galaxy Redshift Survey to study the properties of local radio sources with $S \geq 1$ mJy. 557 objects (hereafter called the spectroscopic sample) drawn from the FIRST survey, corresponding to 2.3 per cent of the total radio sample, are found in the 2dFGRS catalogue within the area $9^h48^m \lesssim$ RA(2000) $\lesssim 14^h32^m$ and $-2°.77 \lesssim$ Dec.(2000) $\lesssim 2°.25$, down to a magnitude limit $b_J = 19.45$. The excellent quality of 2dF spectra allows us to divide these sources into classes, according to their optical spectra.

Absorption-line systems make up 63 per cent of the spectroscopic sample. These may or may not show emission lines due to AGN activity, and correspond to 'classical' radio galaxies belonging mainly to the FRI class. They are characterized by relatively high radio-to-optical ratios, red colours, and high radio luminosities ($10^{21} \lesssim P_{1.4\,GHz}/W\,Hz^{-1}\,sr^{-1} \lesssim 10^{24}$). Actively star-forming galaxies contribute about 32 per cent of the sample. These objects are mainly found at low redshifts ($z \lesssim 0.1$) and show low radio-to-optical ratios, blue colours and low radio luminosities. We also found 18 Seyfert 2 galaxies (3 per cent) and four Seyfert 1s (1 per cent).

Analysis of the local radio luminosity function (LF) shows that radio galaxies are well described by models that assume pure luminosity evolution, at least down to radio powers $P_{1.4\,GHz} \lesssim 10^{20.5}\,W\,Hz^{-1}\,sr^{-1}$. Late-type galaxies, whose relative contribution to the radio LF is found to be lower than was predicted by previous works, present an LF which is comparable with the *IRAS* galaxy LF. This class of sources therefore plausibly constitutes the radio counterpart of the dusty spirals and starbursts that dominate the counts at 60 μm.

[*]E-mail: maglio@sissa.it

1 INTRODUCTION

During the last 20 years, several attempts have been made to model the space density and evolution of radio sources. These attempts have mainly followed two well-defined tracks, where the first class of models (Orr & Browne 1982; Padovani & Urry 1992; Maraschi & Rovetti 1994; Wall & Jackson 1997 – just to mention a few) base their predictions on the unification paradigm which originates from the 'relativistic jet' model of Blandford & Rees (1974), while the second class (Wall, Pearson & Longair 1980; Condon 1984; Danese et al. 1987; Dunlop & Peacock 1990; Rowan-Robinson et al. 1993) relies on the evolutionary properties of the galaxy hosting the radio source.

One of the main limitations affecting both classes of models (especially those from the unification paradigm) is the fact that they were mainly based on data sets including very bright sources ($S_{1.4\,GHz} \simeq 1$ Jy). As a consequence, the low-power tail of the AGN radio luminosity function (LF) is poorly defined, and their predictions at faint flux densities diverge. Some of the models belonging to the second class (e.g. Condon 1984; Danese et al. 1987; Rowan-Robinson et al. 1993) have pushed their analysis down to much lower flux densities ($S \sim 0.1$ mJy), and assume the contribution to the radio population at $S \lesssim 10$ mJy to be principally given by a new class of objects which differs greatly from the radio AGN that dominate at higher fluxes. The limited size of the statistical samples that are available at such faint flux densities means that the nature of this population has remained an issue of debate. For instance, Condon (1984) suggests a population of strongly evolving normal spiral galaxies, while others (Windhorst et al. 1985; Danese et al. 1987; Rowan-Robinson et al. 1993) claim the presence of an actively star-forming galaxy population.

More recently, great efforts have been made to determine the photometric and spectroscopic properties of radio sources at mJy levels and fainter (Georgakakis et al. 1999; Gruppioni, Mignoli & Zamorani 1999; Magliocchetti et al. 2000; Masci et al. 2001). These studies have proven extremely useful in characterizing the populations of radio sources but, once again, the limited statistical samples over small areas of the sky leave significant uncertainties such as the relative contribution of actively star-forming galaxies to the total mJy counts.

The advent of large-area radio surveys which probe the radio sky down to mJy levels (e.g. FIRST, Becker, Helfand & White 1995; NVSS, Condon et al. 1998; SUMSS, Bock, Large & Sadler 1999) overcomes these small-sample limitations which have affected studies of faint radio sources up to now. New studies can be made with multiwavelength follow-ups of large samples of sources drawn from such wide-area surveys. In particular, the acquisition of optical spectra enables us to derive spectral types, luminosity functions (LFs) and redshift distributions for the different radio populations.

The first results in this direction are given by Sadler et al. (1999), who use spectra from the 2dF Galaxy Redshift Survey (Maddox 1998; Colless et al. 2001) to investigate the nature of 127 radio sources drawn from the NVSS down to ~ 2.5 mJy. More recently, this analysis has been extended to include 912 candidate optical counterparts to NVSS sources (Sadler et al. 2002). The present paper follows a similar approach, and presents results for a subsample of 557 sources taken from the FIRST radio catalogue. The FIRST survey includes radio sources that are up to 3 times fainter than those in the NVSS, and the accuracy of the FIRST radio positions is much better than those in the NVSS, which means that the likelihood of correct identifications is significantly improved. On the other hand, the NVSS overlaps a much larger area of the 2dF survey, giving a larger sample of objects to study. For both samples, the 2dF survey spectra provide information on the composition of the radio population associated with optical counterparts brighter than $b_J = 19.45$. Redshift determinations further allow us to estimate quantities such as LFs and redshift distributions for the different classes of sources contributing to the local population (the 2dF Galaxy Redshift Survey samples galaxies up to $z \simeq 0.3$; Colless et al. 2001).

The layout of the paper is as follows. Section 2 briefly introduces the surveys which provided the data (Sections 2.1 and 2.2), and describes the procedure we adopted to obtain the spectroscopic counterparts of a subsample of FIRST radio sources (Section 2.3). Section 3 illustrates the optical and spectroscopic properties of the objects in the sample, while Section 4 deals with their radio properties and presents the results for the local radio LF, obtained by comparing our data with model predictions for different classes of sources. Finally, Section 5 is devoted to the analysis of the observed redshift distributions, and Section 6 summarizes our conclusions. Throughout the paper we will assume $\Omega_0 = 1$ and $h_0 = 0.5$, where $H_0 = h_0 \times 100$ km s^{-1} Mpc^{-1}.

2 THE DATA SETS

2.1 The 2dFGRS

The 2dF Galaxy Redshift Survey (2dFGRS: Maddox 1998; Colless et al. 2001) is a large-scale survey aimed at obtaining spectra for 250 000 galaxies to an extinction-corrected limit for completeness of $b_J = 19.45$ over an area of 2151 square degrees. The survey geometry consists of two broad declination strips, a larger one near the South Galactic Pole (SGP) covering the area $3^h30^m \lesssim$ RA(2000) $\lesssim 21^h40^m$, $-37°.5 \lesssim$ Dec.(2000) $\lesssim -22°.5$ and a smaller one set near the North Galactic Pole (NGP) with $9^h50^m \lesssim$ RA(2000) $\lesssim 14^h50^m$, $2°.5 \lesssim$ Dec.(2000) $\lesssim -7°.5$, plus 100 random 2-degree fields spread uniformly over the 7000 square degrees of the APM catalogue in the southern Galactic hemisphere.

The input catalogue for the survey is a revised version of the APM galaxy catalogue (Maddox et al. 1990a,b, 1996) which includes over 5 million galaxies down to $b_J = 20.5$ in both north and south Galactic hemispheres over a region of almost 10^4 square degrees. The astrometric rms error for galaxies with $17 \le b_J \le 19.5$ is 0.25 arcsec, while the photometry of the catalogue has a precision of about 0.15 mag for galaxies within the same magnitude limits. The mean surface brightness isophotal detection limit of the APM catalogue is $b_J = 25$ mag arcsec^{-2}.

Redshifts z for all the sources brighter than $b_J = 19.45$ are determined in two independent ways, via both cross-correlation of the spectra with specified absorption-line templates (Colless et al. 2001) and by emission-line fitting. These automatic redshift estimates have then been confirmed by visual inspection of each spectrum, and the more reliable of the two results chosen as the

final redshift. A quality flag was assigned to each redshift: $Q = 3$, $Q = 4$ and $Q = 5$ correspond to reliable redshift determinations, $Q = 2$ means a probable redshift, and $Q = 1$ indicates no redshift measurement. The success rate in redshift acquisition for the surveyed galaxies (determined by the inclusion in the 2dF sample of only those objects with quality flags $Q = 3$ to $Q = 5$) is estimated about 95 per cent (Folkes et al. 1999). The median redshift of the galaxies is 0.11, and the great majority have $z < 0.3$. In this work we use the version of the catalogue derived from the 1997 November to 2001 January observations of the north Galactic cap equatorial area, which includes 35 347 galaxies.

2.2 The radio data

The input catalogue for the radio data has been obtained by matching together sources in the FIRST and APM catalogues, as extensively described in Magliocchetti & Maddox (2002).

Briefly, the original radio catalogue comes from the FIRST (Faint Images of the Radio Sky at Twenty centimetres) survey (Becker et al. 1995). The latest release (2000 July 5) of the catalogue covers about 7988 square degrees of the sky in the north Galactic cap and equatorial zones, including most of the area $7^h20^m \lesssim RA(2000) \lesssim 17^h20^m$, $22°.2 \lesssim Dec.(2000) \lesssim 57°.5$ and $21^h20^m \lesssim RA(2000) \lesssim 3^h20^m$, $-2°.8 \lesssim Dec.(2000) \lesssim 2°.2$, and comprises approximately 722 354 sources down to a flux limit $S_{1.4\,GHz} \simeq 0.8\,mJy$, with a 5σ source detection limit of $\sim 1\,mJy$. The catalogue has been estimated to be 95 per cent complete at 2 mJy, and 80 per cent complete at 1 mJy (Becker et al. 1995).

Optical counterparts for a subsample of FIRST radio sources have then been obtained by matching together objects included in the radio catalogue with objects coming from the APM survey. Since the APM and FIRST surveys overlap only in a relatively small region of the sky on the equatorial plane between $9^h48^m \lesssim RA(2000) \lesssim 14^h32^m$ and $-2°.77 \lesssim Dec.(2000) \lesssim 2°.25$, the search for optical counterparts was restricted to this area.

Out of approximately 24 000 radio sources with $S \geq 1\,mJy$ in the considered area, Magliocchetti & Maddox (2002) find 4075 identifications – corresponding to 16.7 per cent of the original sample – in the APM catalogue for $b_J \leq 22$ and for a matching radius of 2 arcsec. This last value was chosen after a careful analysis of the distribution of the residuals $\Delta x = x_{RADIO} - x_{OPTICAL}$, $\Delta y = y_{RADIO} - y_{OPTICAL}$ between the positions of radio and optical sources. The rms value of the $\Delta x - \Delta y$ distribution is found to be 0.7 arcsec, which is consistent with the uncertainty obtained by summing the positional uncertainties of the FIRST (~ 0.5 arcsec) and APM (~ 0.5 arcsec) surveys in quadrature and taking into account a small distortion between the radio and optical reference frames. So a 2-arcsec match radius is equivalent to about 2.5σ, which should include ~ 97 per cent of the true identifications. Furthermore, using this match radius limits the number of random coincidences to a negligible ~ 5 per cent (225 sources out of 4075). To ensure uniform completeness over the optical survey, we restricted the analysis to objects with $b_J \leq 21.5$, leading to 3176 identifications.

Since the adopted version of the APM data includes magnitude measurements only in the b_j band, R magnitudes were then assigned to the optical identifications by making use of the $b_J - R$ colour estimates given in APMCAT (found online at *http://www.ast.cam.ac.uk/~apmcat* Irwin et al.). This version of the APM data has been processed to provide accurate stellar magnitudes, and so the galaxy magnitudes are not so reliable, but it does include both R and b_j UKST plates. Since the data are not designed for galaxy

work, these colours have a rather large uncertainty, but nevertheless provide interesting information.

In the magnitude range $16 \leq b_J \leq 20.5$ image profiles were used to separate galaxies from stars as described by Maddox et al. (1990a). For $b_J \gtrsim 20.5$ galaxy profiles do not greatly differ from stellar profiles, and the classification becomes unreliable. So, for $16 \leq b_J \leq 20.5$ we divide the radio sources into stellar-like objects, expected to be mostly high-redshift QSOs (535 objects) and radio galaxies (1494 objects), expected to lie within $z \simeq 0.3$. The radio-to-optical ratios and colours of the stellar identifications are consistent with them being mostly high-redshift QSOs.

2.3 The spectroscopic sample

In order to obtain redshift measurements and spectral features for those radio sources with an optical counterpart (hereafter called the photometric sample) as described in Section 2.2, we looked for objects in the 2dF catalogue with positions which differed by less than 2 arcsec from positions of sources in the photometric sample. The choice of this value for the matching radius is based on the 2-arcsec diameter of each 2dF fibre. Indeed, we found all the matched objects to have positional offsets of maximum 1 arcsec, with a rms of ~ 0.5 arcsec. Fig. 1 shows the distribution of the residuals $\Delta x = x_{OPT} - x_{SPEC}$, $\Delta y = y_{OPT} - y_{SPEC}$ between the positions of sources in the photometric and 2dF catalogues. The bottom panel represents the $\Delta x - \Delta y$ distribution, while the middle and top panels show the number of matches respectively as a function of Δx and Δy offsets. As already discussed, all the offsets lie within $\Delta x \simeq \Delta y \sim 1$, with ~ 0.5 arcsec rms. The shift of the median offset of the distribution from the zero values, more prominent along the Δy-axis, is due to adjustments in the astrometry for galaxies in the 2dF survey relative to those included in the earlier version of the APM catalogue from which the photometric sample was drawn.

Out of 971 input sources from the photometric catalogue with $b_J \leq 19.45$ and $S \geq 1\,mJy$, we were then able to obtain redshifts for 557 objects, 53 per cent of the original sample. Fig. 2 shows the projected distribution of radio sources in the photometric sample with $b_J \leq 19.45$; filled circles identify those objects for which redshift estimates and spectral classifications were available. We

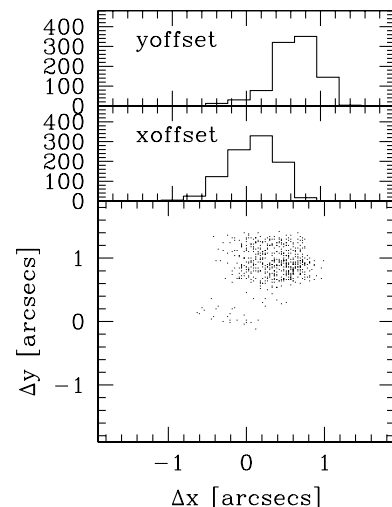**Figure 1.** Bottom panel: distribution of the residuals $\Delta x = x_{OPT} - x_{SPEC}$, $\Delta y = y_{OPT} - y_{SPEC}$ between optical and spectroscopic positions. Middle and top panels: number of matches as a function of Δx and Δy offsets.
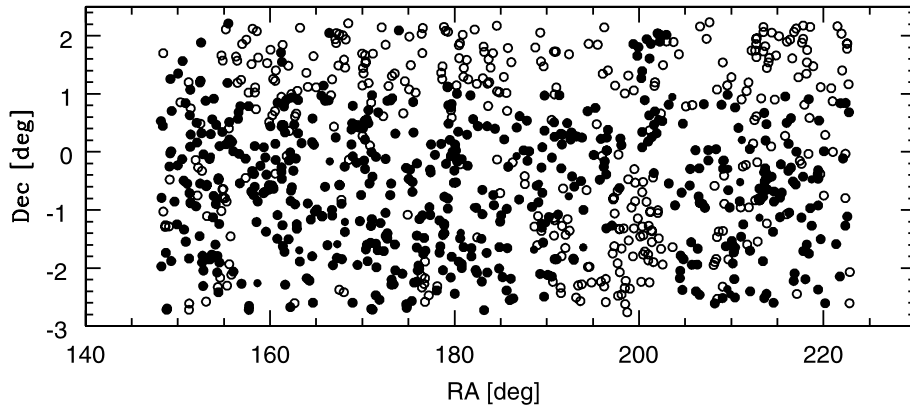
Figure 2. Projected distribution of radio sources with optical counterparts in the APM catalogue with $b_J \leq 19.45$. Filled circles identify objects with spectral identifications, while empty ones are for those not yet included in the 2dFGRS.
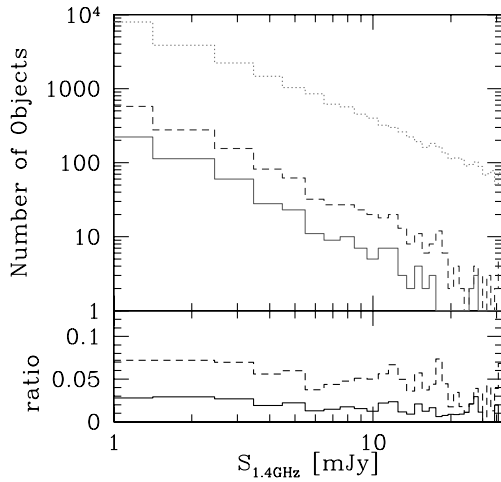

Figure 3. Number of radio sources per flux interval in the considered area. The dotted line represents the original radio sample, and the dashed line those sources with optical counterparts brighter than $b_J \leq 22$ (photometric sample), while the solid line is for sources with spectral determinations from the 2dFGRS (spectroscopic sample). The lower panel represents the ratio between the number of sources respectively in the spectroscopic and radio sample (solid line) and optical and radio sample (dashed line) as a function of radio flux.

Figure 4. Number of radio sources per magnitude interval over the considered area. The dashed line represents sources from the photometric sample, while the solid line is for sources with spectral determinations from the 2dFGRS (spectroscopic sample). The lower panel represents the ratio between the number of sources respectively in the spectroscopic and photometric sample as a function of magnitude.

remark here that the reason for such an apparent incompleteness in the redshift determination is mainly the incompleteness of the sky coverage, as there are areas which have not yet been observed by the 2dFGRS. Less that 40 objects from the input sample with $b_J \leq 19.45$ could in fact have been missed due to the completeness level of the redshift survey (~95 per cent; Colless et al. 2001).

To test for both radio-flux and magnitude biases in the determination of the photometric and spectroscopic samples, we show the number of radio sources respectively per flux and magnitude unit in Figs 3 and 4. In Fig. 3, the dotted line has been obtained from the original FIRST catalogue for all those sources enclosed in the equatorial region defined in Section 2, while the dashed line illustrates the case for the photometric sample ($b_J \leq 20.5$), and the solid line represents the spectroscopic sample. In Fig. 4, the dashed and solid lines are for the photometric and spectroscopic samples respectively. In each figure the lower panel shows the ratio of number counts in each sample. The ratio of spectroscopic to photometric sources remains constant with

magnitude up to $b_J \sim 19$–19.5, but there is a weak trend for there to be more identifications at faint radio fluxes. It is not entirely clear what causes this trend; one possibility could be the fact that fainter optical objects are in general associated with brighter radio sources (e.g., high-z ellipticals – see later in Sections 3 and 4). Whatever the reason, we can confidently exclude the presence of any strong bias in the radio-flux or magnitude distribution, first of all for the optical counterparts of radio sources (as already discussed in Magliocchetti & Maddox 2002) and also for the subset for which we have their redshifts. As a final remark, note that Fig. 4 shows a tendency for the number of sources both in the photometric and spectroscopic samples to flatten for magnitudes $b_J \gtrsim 17.5$. As will be discussed in Section 4, this behaviour is due to the absence of optically faint star-forming galaxies in the FIRST survey.

Before carrying on with our analysis, it is worthwhile mentioning an important issue which needs to be taken into account when dealing with objects coming from the FIRST survey related to flux measurements. The high resolution of the survey in fact implies that some of the flux coming from extended sources

could be either resolved out or split into two or more components, leading to a systematic underestimate of the real flux densities of such sources (Condon et al. 1998). This effect has been partially corrected for by using the method developed by Magliocchetti et al. (1998) to combine multicomponent sources. However, despite this correction, it turns out that fluxes as derived from the FIRST survey were on average still lower than those measured by the NVSS survey (which, having a lower resolution, should not be affected by this effect) by about 1 mJy in the case of sources brighter than 3 mJy, and by about 30 per cent of the measured flux for sources with $1\,\mathrm{mJy} \lesssim S_{1.4\,\mathrm{GHz}} \lesssim 3\,\mathrm{mJy}$ (Jackson et al. in preparation). We therefore corrected the estimated flux densities by making use of the above quantities and, while for consistency reasons throughout the paper we will keep using the flux densities as measured by the FIRST survey, in the calculation of high-precision quantities such as the RLF (see Section 4), we will rely on these corrected values. It is nevertheless worth stressing that such corrections do not affect any of the results presented in this paper (including the LFs) by more than a negligible factor, generally much lower than other uncertainties associated with the various measurements.

3 OPTICAL AND SPECTRAL PROPERTIES OF THE SAMPLE

All the 557 radio sources identified in the 2dF catalogue are presented in Tables 2 and 3 at the end of the paper. For each object the tables indicate the following.

(1) Source number.

(2) Right Ascension α (J2000) and Declination δ (J2000). Note that these correspond to the FIRST radio coordinates, except in the case of objects with double or triple substructures, where the coordinates are of the centroid of the source and are obtained by following the procedure illustrated by Magliocchetti et al. (1998) to combine multicomponent objects.

(3) Offset (expressed in arcsecs) of the optical counterpart in the APM catalogue.

(4) Radio-flux density (in mJy units) at 1.4 GHz.

(5) Apparent b_J and, when present,

(6) R magnitude of the optical counterpart.

(7) Redshift.

(8) Spectral classification. It is worth remarking here that, as Madgwick et al. (2002) have recently shown, the fibre spectral classification inconsistency claimed by Kochanek, Pahre & Falco (2002) is not a problem for 2dFGRS. We refer the reader to Madgwick et al. for further discussion on this point.

(9) Emission lines detected ordered from the most to the least prominent. Note that the [N II] line appears in the tables only if its intensity is comparable with that of Hα.

(10) Notes on morphological appearance.

The point (10) has been obtained by visual inspection of the radio (R, from the FIRST atlas) and optical (O, from the Digitized Sky Survey) images of each source. Blank spaces correspond to point-like structures as observed both in the radio and optical bands. Radio images have been classified as *Extended* whenever it was possible to detect any extended structure, *Double* if the source presented the two characteristic lobes, *Core + lobes* if also the central component of the radio source was present, and *Jets/Core + Jets* if the structures pointing towards the lobes were visible. In a few cases, the '?' indicates uncertainty to distinguish

between genuine double/triple structures and the presence of side-lobes.

From the optical point of view, galaxies have been classified as *Spiral* whenever the presence of spiral arms was visible or *Disk + bulge* if the image clearly resolved the galaxy into the two components, *Irregular* if they presented distorted morphologies, *Merging* if there were signatures of either merging or accretion of a smaller unit, and *Interaction* whenever two or more galaxies were interacting with each other. Again, the '?' indicates dubious classifications.

Classes for the optical counterparts of radio sources (column 10 of Tables 2 and 3) have been assigned on the basis of their 2dF spectra. Spectra have been compared with known templates (see, e.g., Kennicutt 1992 and McQuade, Calzetti & Kinney 1995), and this allowed galaxies to be divided into six broad categories.

(1) *Early-type galaxies*, where spectra were dominated by continua much stronger than the intensity of any emission line. These objects can be further divided into two sub-classes:

(i) galaxies with absorption lines only, and

(ii) galaxies with absorption lines + weak [O II] and Hα emission lines denoting little star formation activity.

(2) *E + AGN-type galaxies*, showing spectra typical of early-types plus the presence of (narrow) emission lines such as [O II], [O III], [N II] and [S II], which are strong if compared to any Balmer line in emission and indicate the presence of large, partially ionized transition regions, as is the case in active galaxies.

(3) *Late-type galaxies*, where spectra show strong emission (mainly Balmer) lines characteristic of star formation activity, together with a detectable continuum.

(4) *Starburst (SB) galaxies*, with optical spectra characterized by an almost negligible continuum with very strong emission lines indicating the presence of intense star formation activity.

(5) *Seyfert 1 galaxies*, with spectra showing strong, broad emission lines.

(6) *Seyfert 2 galaxies*, where the continuum is missing and spectra show only strong narrow emission lines due to the presence of an active galactic nucleus.

Lastly, we also found three Galactic stars, probably due to random positional coincidences with extragalactic radio sources.

Distinctions amongst different classes of sources, and in particular amongst E + AGN, Seyfert 2 and late-type galaxies, have relied on the diagnostic emission-line ratios of Veilleux & Osterbrock (1987), Woltjer (1990) and Rola, Terlevich & Terlevich (1997) (where this last approach, based on the relative intensity of Hβ, has been adopted whenever the Hα line would fall off the spectrum, i.e., for $z \gtrsim 0.2$). Note that a definite classification was not possible for all the cases. This simply reflects the fact that it is in general quite common to find 'composite' galaxies containing both an AGN and ongoing star formation (see, e.g., Hill et al. 2001).

The photometric properties of the different classes which constitute the spectroscopic sample are illustrated by Figs 5 and 6. In all the plots, symbols are as follows: empty circles for early-type galaxies, filled ones for E + AGN, filled triangles for late-type galaxies, filled squares for starbursts, empty squares for Seyfert 2, and crosses for Seyfert 1 objects. Note that we did not include here the small number of uncertain classification sources.

Fig. 5 respectively shows b_J magnitudes versus radio flux S at 1.4 GHz (upper panels) and redshift (lower panels) for the different classes of objects in the spectroscopic sample; left-hand panels are for early and E + AGN galaxies, middle panels are for late-type
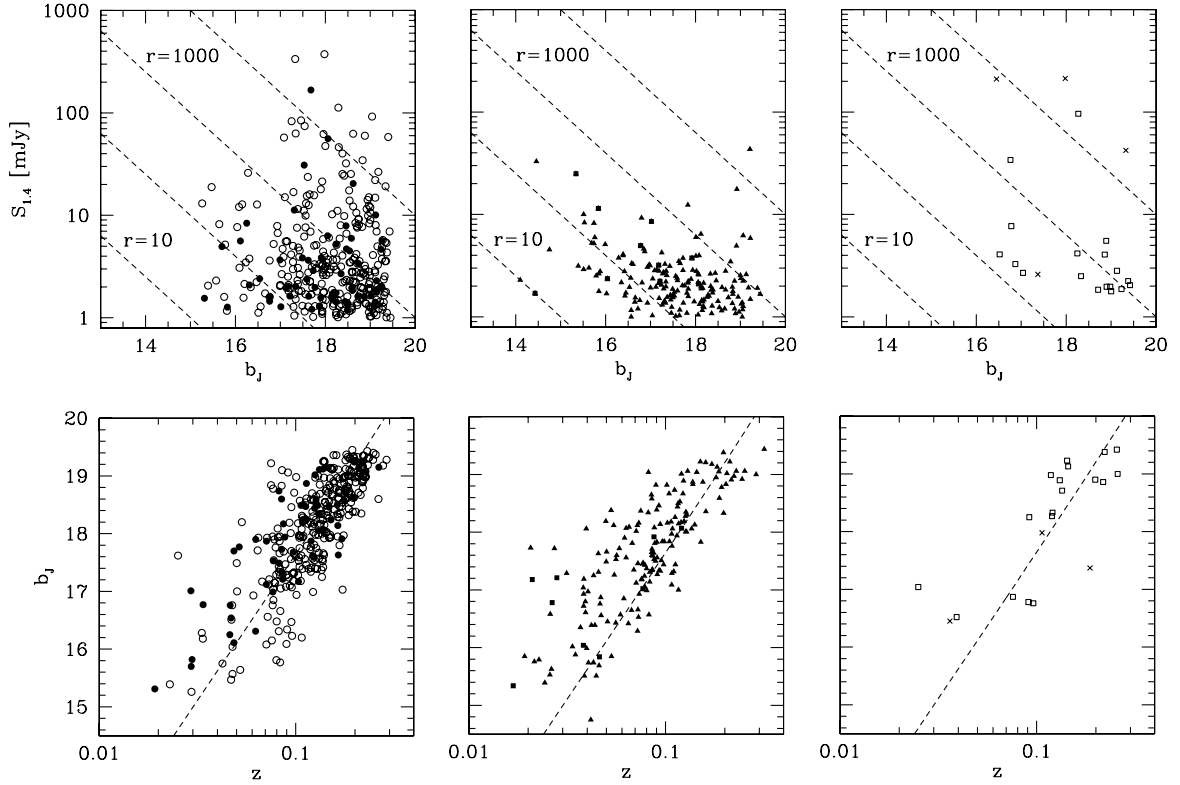
Figure 5. b_J magnitudes versus radio flux S at 1.4 GHz (upper panels) and redshift (lower panels) for the different classes of objects discussed in the paper. From left to right, plots are derived for early-type (represented by empty circles) and E + AGN (filled circles) galaxies, late-type (filled triangles) and starburst (filled squares) galaxies and Seyfert 1/Seyfert 2 (respectively illustrated by crosses and empty squares) objects. The few uncertain classification sources are not included in the plots. The dashed lines in the upper panels correspond to constant values of the radio-to-optical ratios $r = 1, 10, 100, 10^3$ and 10^4, while those in the b_J-z plots represent the best fit to the data obtained for the population of early-type galaxies, corresponding to an absolute magnitude $M_B = -21.3$ (see text for details).

and starburst galaxies, while the right-hand panels represent the populations of Seyfert 1 and Seyfert 2 galaxies. The dashed lines (in the upper panels) indicate the loci of constant radio-to-optical ratios $r = S \times 10^{(m-12.5)/2.5}$, where S is expressed in mJy, and $m \equiv b_J$. Note that $R - z$ and $R - S$ trends for the different classes of sources are not presented here, as they simply reproduce the same features as those already shown in Fig. 5. Fig. 6 instead represents $b_J - R$ colours for the different populations as a function of radio flux S (upper panels) and redshift (lower panels). Symbols are as in Fig. 5.

As one can notice from Figs 5 and 6, different classes of objects occupy different regions on the various $S - b_J$, b_J-z, etc. planes; this is due to intrinsic characteristics of the various populations which we summarize here.

(1) Early-type galaxies.

This class comprises 289 objects and makes up 52 per cent of the whole spectroscopic sample. On average, sources belonging to this population have relatively high values for the radio-to-optical ratio ($100 \lesssim r \lesssim 10^4$) and are preferentially found at redshifts $z \gtrsim 0.1$. The majority of these sources show rather red colours ($b_J - R \gtrsim 1$), with a tendency to be redder at larger look-back times. Their radio fluxes lie in the range $1 \lesssim S/\text{mJy} \lesssim 10$, even though objects are found up to $S \sim 400$ mJy, and optically they appear as relatively faint (about 60 per cent of the sources has $b_J \gtrsim 18$). The b_J-z relation in this case (represented by the dashed line in the lower left panel of Fig. 5) is well described by the relation

$$b_J - M_B = -5 + 5\log_{10}d_L(\text{pc})$$

$$\simeq 25 - 5\log_{10}\text{H}_0 + 5\log cz + 1.086(1 - q_0)z \quad (1)$$

(d_L is the luminosity distance, $q_0 = \Omega_0/2$, and M_B is the absolute magnitude in the b_J-band). A χ^2 fit to the data performed with M_B as free parameter gives, for an $h_0 = 0.5$, $\Omega_0 = 1$ universe, $M_B = -21.29$ with little scatter about this value ($\Delta M_B = 0.28$ mag). This result is in very good agreement with previous estimates (see, e.g., Rixon, Benn & Wall 1991, Georgakakis et al. 1999, Gruppioni et al. 1999 and Magliocchetti et al. 2000), showing that passive radio galaxies are reliable standard candles.

(2) E + AGN galaxies.

There are 61 objects in this class, corresponding to 11 per cent of the spectroscopic sample. These sources are directly connected to the class of early-type galaxies, even though they show characteristics that are intermediate between pure AGN-fuelled sources and star-forming galaxies. Optically they appear as rather faint, and they closely follow the standard-candle relationship found for early-type galaxies ($M_B = -21.45 \pm 0.41$ mag). However, their radio-to-optical ratios are in general as low as those obtained for late-type galaxies. Their radio fluxes are in general quite low ($S \lesssim 5$ mJy), and their $b_J - R$ colours are uniformly distributed between about 0 and 2.

(3) Late-type galaxies and starbursts.

This class comprises 177 objects (including 10 SB), which is ~ 30 per cent of the spectroscopic sample. The radio-to-optical ratios r for these sources have values between 60 and 10^3, in general smaller than those found for early-type galaxies. Their radio fluxes are rarely brighter than $S \simeq 5$ mJy, and optically they have bright apparent magnitudes (very few objects are found with $b_J \gtrsim 18.5$). These sources have quite blue colours, $-2 \lesssim b_J - R \lesssim 1$, and are mostly local – the majority of them being found within $z \simeq 0.1$.
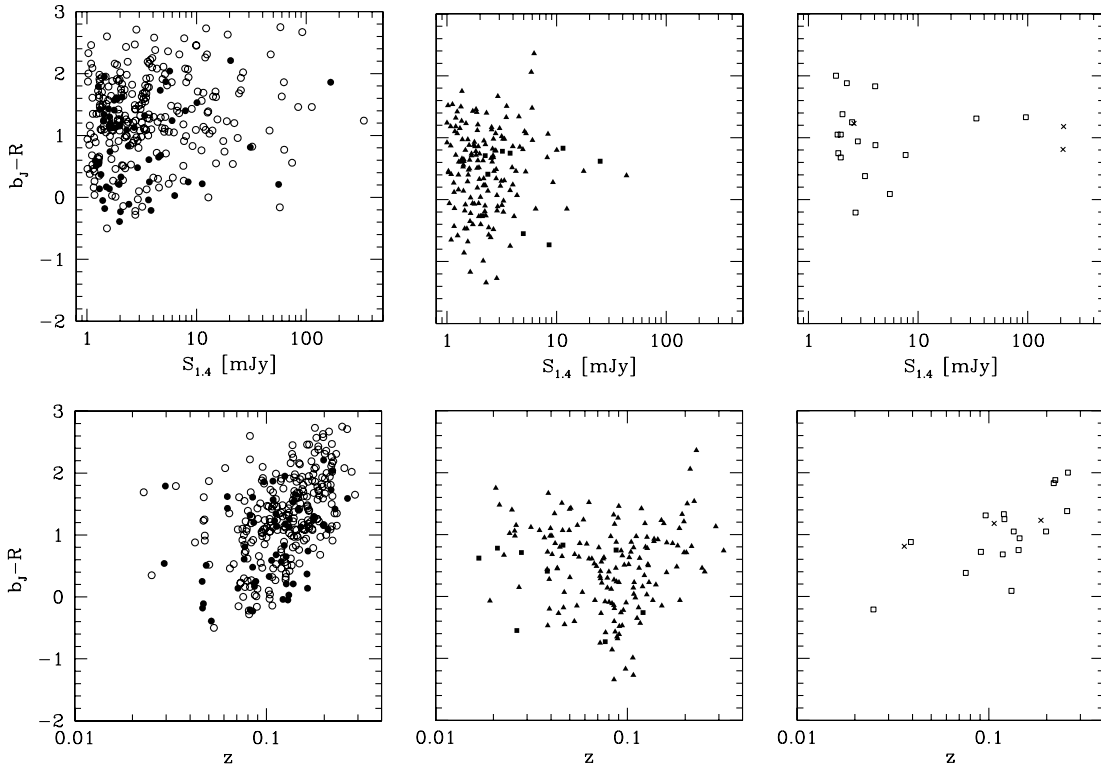
Figure 6. Upper panels: $b_J - R$ colours for the different classes of sources as a function of radio flux at 1.4 GHz, S. Lower panels: $b_J - R$ colours as a function of redshift. Empty circles represent early-type galaxies, filled circles are for E + AGN, filled triangles are for late-type galaxies, filled squares are for starbursts, empty squares are for Seyfert 2, and crosses illustrate the case of Seyfert 1 objects.

Furthermore, they do not follow the $b_J - z$ relation found for early-type galaxies, illustrated by the dashed line in the lower middle panel of Fig. 5. For these objects one in fact finds $M_B = -20.76 \pm 0.33$ mag.

(4) Seyfert galaxies.
The sample contains 18 Seyfert 2 and four Seyfert 1 galaxies, making up ~ 3 and 0.5 per cent of the sample respectively. Their radio-to-optical ratios are quite high, and in the case of all but one Seyfert 1 galaxy, one finds $r \gtrsim 10^4$. Their colours range between $0 \lesssim b_J - R \lesssim 2$ as in the case for E + AGN galaxies, and they seem to follow the $b_J - z$ relationship found for early-type galaxies (lower left panel of Fig. 5). Seyfert 2 galaxies in general have low-to-intermediate radio fluxes, while Seyfert 1s show higher values for S. Note that one Seyfert 1 galaxy (number 331 437 of the spectroscopic sample) is found at $z = 2.24$, well beyond the typical limit of the 2dFGRS, $z \simeq 0.3$.

The above findings for the relative contribution of the different classes of sources to the local radio population are in good general agreement with the results of Sadler et al. (2002) for a sample of NVSS/2dFGRS galaxies. However, Sadler et al. (2002) find approximately 40 per cent are star-forming galaxies, the increased fraction almost certainly being due to the lower resolution of the NVSS which will detect (or catalogue) low surface brightness sources at the lowest flux densities.

Some information on the above classes of sources can also be derived from the few optical images showing resolved structures. For instance, it is interesting to note that the majority of the interacting/merging systems seem to be associated with early-type spectra, typical of pure AGN-fuelled sources, suggesting that merging, under appropriate conditions, can trigger AGN activity even at low redshifts. Also, as expected, irregulars and spirals
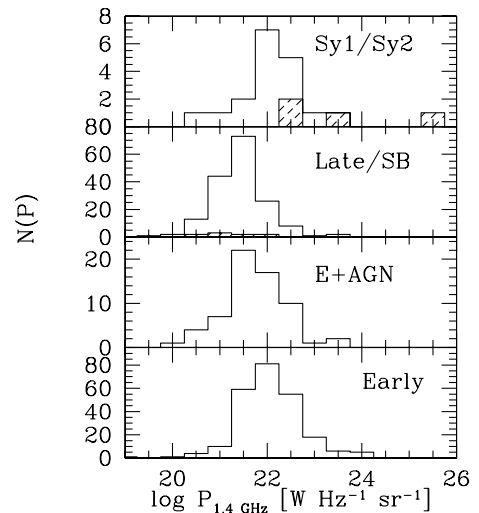
Figure 7. Distribution of monochromatic radio power at 1.4 GHz for the six classes of sources discussed in the paper. In the first and second panels from top, shaded histograms respectively illustrate the distribution of Seyfert 1 galaxies and starbursts (not clearly seen due to the small number of sources).

preferentially show spectra typical of late-type galaxies; signatures of interaction and/or merging are seen for members of this latter population as well as for E + AGN galaxies. Interaction/merging is also observed for one of the four Seyfert 1 galaxies and two Seyfert 2s. Furthermore, we find one Seyfert 2 to be associated to the classical two-lobed radio image.

Note that in a few cases, early-type/E + AGN galaxies are found to correspond to spiral morphologies. This is simply due to our

classification criteria, which are based solely on the spectra; typical spectra of Sab spiral galaxies can be very similar to early-type galaxies with [O II] and Hα emission lines. Finally, radio images show that there is a clear trend for extended/substructured sources to be associated with absorption systems (i.e., early-type galaxies).

4 RADIO PROPERTIES OF THE SAMPLE

More information on the nature of the sources in the spectroscopic sample can be inferred by investigating radio properties such as the distribution of their radio powers and the radio luminosity function (hereafter denoted as LF).

From investigation of the radio-flux distribution as a function of redshift for the different populations as inferred from Fig. 5 (upper and lower panels), we note that in general Seyfert 1 and early-type galaxies show higher radio fluxes compared to the other classes of sources. There is also a tendency for late-type and SB galaxies to be present only in the local Universe, as already mentioned. No other distinction amongst the different populations is evident in the data.

Radio powers have been calculated according to the relation $P_{1.4\,GHz} = S_{1.4\,GHz}D^2(1 + z)^{3+\alpha}$, and are expressed in $W\,Hz^{-1}\,sr^{-1}$ units. In the above formula, D is the angular diameter distance, and α is the spectral index of the radio emission $[S(\nu) \propto \nu^{-\alpha}]$. As we did not have measured values for this latter quantity, we assumed $\alpha = 0.5$ for Seyfert 1 galaxies, $\alpha = 0.75$ for early-type galaxies (with or without emission lines due to AGN activity), $\alpha = 0.7$ for Seyfert 2s, and $\alpha = 0.35$ both for late-type galaxies and starbursts (see, e.g., Oort, Steemers & Windhorst 1988). Note, however, that, since the redshift range is relatively small, the results do not depend on the precise values of the spectral index. Fig. 7 shows the distribution of radio luminosities for the different classes of sources. In the top panel, the shaded histogram corresponds to the distribution of Seyfert 1 galaxies, while in the second panel from the top it represents the population of SB galaxies (not very clearly seen due to the small number of sources). As one can see from the figure, early-type galaxies show generally higher radio powers ($10^{21} \lesssim P_{1.4\,GHz}/W\,Hz^{-1}\,sr^{-1} \lesssim 10^{23}$, extending up to $10^{24}\,W\,Hz^{-1}\,sr^{-1}$) than late-type ones, whose majority presents $P_{1.4\,GHz} \lesssim 10^{21.5}\,W\,Hz^{-1}\,sr^{-1}$. E + AGN sources are instead characterized by luminosities with values closer to those found for early-type galaxies ($10^{20} \lesssim P_{1.4\,GHz}\,W\,Hz^{-1}\,sr^{-1} \lesssim 10^{22.5}$). The bulk of the Seyfert 2 distribution is obtained for $P_{1.4\,GHz} \simeq 10^{22}\,W\,Hz^{-1}\,sr^{-1}$, while Seyfert 1 galaxies all have $P_{1.4\,GHz} \gtrsim 10^{22.5}\,W\,Hz^{-1}\,sr^{-1}$. We note that the apparent cut in the luminosity distribution at $P_{1.4\,GHz} \simeq 10^{20}\,W\,Hz^{-1}\,sr^{-1}$ is simply due to the 1 mJy limit adopted for sources in the original radio sample ($S = 1$ mJy corresponds to $P_{1.4\,GHz} \simeq 10^{20}\,W\,Hz^{-1}\,sr^{-1}$ for $z = 0.02$, redshift of the nearest object in the spectroscopic sample).

It is worth remarking here that all the objects included in the spectroscopic sample (apart from the one Seyfert 1 found at $z = 2.24$) have $P_{1.4\,GHz} \lesssim 10^{24}\,W\,Hz^{-1}\,sr^{-1}$. In the case of 'classical' radio sources (i.e., if one excludes late-type galaxies and starbursts from the analysis, since the radio signal stems from non-AGN activity) this implies that the overwhelming majority of early and E + AGN galaxies belong to the class of FR I sources (Fanaroff & Riley 1974). In fact, although the distinction between FR I and FR II sources seems to be more complicated than just based on their radio power – as in general optically brighter FR I also tend to appear as more luminous in the radio band (see, e.g., Ledlow &

Owen 1996) – we note that for $P_{1.4\,GHz} \lesssim 10^{24}\,W\,Hz^{-1}\,sr^{-1}$ only members of FR I are found, independent of their magnitude.

Also, from a morphological point of view, we find that very few objects in the sample (about 5 per cent) show composite structures such as lobes or jets. The angular resolution of the FIRST survey is about 5 arcsec which, for the cosmology adopted in this paper, corresponds to a physical scale of ~ 7 kpc at $z = 0.05$ and ~ 35 kpc at $z = 0.3$ (the maximum redshift found for galaxies in the 2dFGRS). Thus, for all the sources showing point-like images in the radio, one can exclude the presence of very extended structures such as those typical of FR II sources.

The local radio LF for objects in the spectroscopic sample has then been derived by grouping the sources in bins of width $\Delta \log_{10}P = 0.4$, according to the expression

$$\Phi(P) = \sum_i N_i(P, P + \Delta P)/V_{max}^i(P), \qquad (2)$$

where N_i is the number of objects with luminosities between P and $P + \Delta P$, and $V_{max}^i(P)$ is the maximum comoving volume within which an object could have been detected above the radio-flux and magnitude limits of the survey (Rowan-Robinson 1968). As already stated in Section 2, for the radio-flux limit we set $S = 1$ mJy, the value at which the incompleteness of the original radio catalogue has been well assessed to be ~ 20 per cent, while $b_J = 19.45$ (derived for 2dFGRS galaxies) is the chosen magnitude limit. Note that this value could be transformed into a rough redshift estimate for completeness of the spectroscopic sample, $z \simeq 0.2$, under the assumption of radio galaxies as standard candles with $M_B \simeq -21.3$ (see equation 1 and Fig. 5).

For each source we then estimated the maximum redshift at which it could have been included in the sample, $z_{max} = \min(z_{max}^R, z_{max}^O)$, where z_{max}^R and z_{max}^O are the redshifts at which the source would disappear from the sample respectively due to radio and optical limiting flux densities. For the optical k-corrections we adopted, under the assumption of spectra of the form $S \propto \nu^{-\alpha_{opt}}$, $\alpha_{opt} = 5$ for early-type galaxies, $\alpha_{opt} = 3$ for late-type galaxies, and $\alpha_{opt} = 0.5$ for Seyferts (both type 1 and 2; see Rowan-Robinson et al. 1993).

In principle, in order to derive the local LF, one should de-evolve the luminosity of each source at $z = 0$ according to expressions such as $P(0) = P(z) \exp^{-t(z)/\tau}$ (where in this case we assumed pure luminosity evolution), where $t(z)$ is the look-back time in units of the Hubble time, and τ is the time-scale of the evolution in the same units. However, given the limited redshift range spanned by the sources in the spectroscopic sample, we assumed no evolution (i.e., $\tau \to \infty$) for all the classes of objects, and therefore set $P(0) \equiv P(z)$.

The values for the LF obtained as in equation (2) have then been corrected respectively by means of the factor $0.8 \times 556/971$ to take into account the 80 per cent completeness of the FIRST survey for sources between 1 and 2 mJy, $0.95 \times 556/971$ for sources between 2 and 3 mJy, and simply $556/971$ for sources brighter than 3 mJy (see Becker et al. 1995), where the ratio $556/971$ indicates the fraction of objects with $b_J \leq 19.45$ observed by the 2dFGRS in the considered area (see Section 2.3), and reported in Table 1 (first column).

Fig. 8 shows the results for the whole spectroscopic sample, with error bars showing the Poisson errors. The dashed line indicates the prediction from Rowan-Robinson et al. (1993), who consider a luminosity function of the form

$$\Phi(P, z) = \Phi_{SP}(P) + \Phi_{ELL}(P, z), \qquad (3)$$

Table 1. The local radio luminosity function at 1.4 GHz in Mpc^{-1} $\Delta\log_{10}P$ units. Luminosities are expressed in W Hz^{-1} sr^{-1}.

$\log_{10}P$	Complete sample		Early-type		E/E + AGN		Late-type	
	$\log_{10}\Phi$	N_{All}	$\log_{10}\Phi$	N_{Early}	$\log_{10}\Phi$	$N_{\text{E/E+AGN}}$	$\log_{10}\Phi$	N_{Late}
20.6	-3.79 ± 0.15	8	-4.46 ± 0.30	2	-4.03 ± 0.19	5	-4.16 ± 0.25	3
21.0	-3.85 ± 0.08	29	-4.76 ± 0.21	4	-4.51 ± 0.16	7	-3.96 ± 0.09	22
21.4	-4.16 ± 0.05	57	-4.81 ± 0.13	11	-4.64 ± 0.10	17	-4.34 ± 0.07	39
21.8	-4.30 ± 0.04	131	-4.71 ± 0.06	49	-4.60 ± 0.05	65	-4.59 ± 0.05	66
22.2	-4.67 ± 0.04	132	-4.91 ± 0.05	81	-4.81 ± 0.04	98	-5.32 ± 0.08	28
22.6	-4.98 ± 0.04	102	-5.12 ± 0.05	74	-5.06 ± 0.05	84	-5.98 ± 0.12	12
23.0	-5.25 ± 0.06	53	-5.41 ± 0.07	38	-5.33 ± 0.06	44	-6.48 ± 0.18	6
23.4	-5.73 ± 0.09	21	-5.76 ± 0.10	19	-5.73 ± 0.09	21		
23.8	-5.97 ± 0.13	11	-6.36 ± 0.17	6	-6.24 ± 0.16	7	-6.67 ± 0.31	2
24.2	-6.51 ± 0.21	4	-6.51 ± 0.21	4	-6.51 ± 0.21	4		
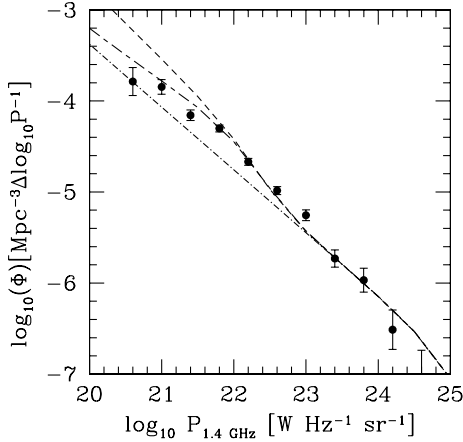
Figure 8. Local radio luminosity function at 1.4 GHz for all the objects in the spectroscopic sample with $S \geq 1$ mJy and $b_J \leq 19.45$. The dashed line indicates the prediction from Rowan-Robinson et al. (1993), while the dot-dashed line represents the predicted LF for the population of AGN-fuelled steep-spectrum sources as given by Dunlop & Peacock (1990) under the hypothesis of pure luminosity evolution. The long/short-dashed line is obtained from equations (3), (4) and (5) for $P_* = 10^{21.7}$ W Hz^{-1} sr^{-1}, $\beta = 1.4$, $C = 0.425 \times 10^{-4}$ and $\sigma = 0.44$ (see text for details).

where

$$\Phi_{\text{ELL}}(P,z) = \frac{10^{-6.91}}{[P_{1.4}/P_{\text{c}}(z)]^{0.69} + [P_{1.4}/P_{\text{c}}(z)]^{2.17}} \quad (4)$$

(illustrated in Fig. 8 by the dot-dashed line) is the LF for steep-spectrum FR I + FR II sources as given by Dunlop & Peacock (1990) under the assumption of pure luminosity evolution. The evolving 'break' luminosity is given by $\log_{10}P_{\text{c}}(z) = 25.12 + 1.26z - 0.26z^2$ (in W Hz^{-1} sr^{-1} units) which, since we have assumed no evolution, reduces to the value corresponding to $z = 0$, and

$$\Phi_{\text{SP}}(P) = C\left(\frac{P}{P_*}\right)^{1-\beta} \exp\left\{-\frac{\left[\log_{10}\left(1+\frac{P}{P_*}\right)\right]^2}{2\sigma^2}\right\}, \quad (5)$$

with $C = 0.425 \times 10^{-4}$, $\log_{10}P_* = 21.83$ W Hz^{-1} sr^{-1},[1] $\beta = 1.82$, $\sigma = 0.44$, is the luminosity function for the population of spirals/starbursting galaxies as derived for *IRAS* sources by

[1] This value has been obtained after correcting the typing error in Rowan-Robinson et al. (1993; Rowan-Robinson, private communication).
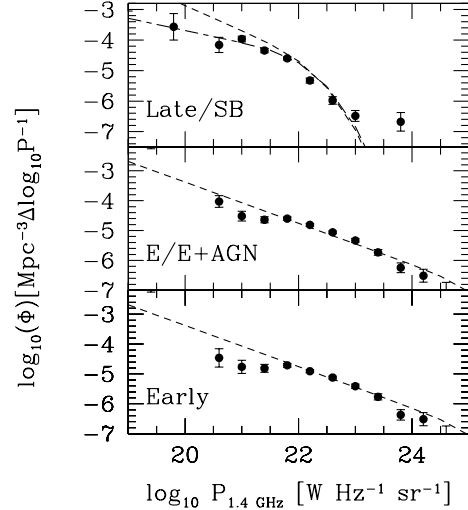
Figure 9. Local radio luminosity function at 1.4 GHz for late-type+SB galaxies (top panel), early and E + AGN galaxies (middle panel) and early-type galaxies only (bottom panel). All the sources have $b_J \leq 19.45$, completeness limit of the spectroscopic sample, and $S \geq 1$ mJy. The dashed lines in the middle and bottom panels indicate the Dunlop & Peacock (1990) model for pure luminosity evolution for the population of AGN-fuelled, steep-spectrum sources, while the one in the top panel represents the prediction from Rowan-Robinson et al. (1993) for spirals/starburst galaxies. The long/short-dashed line is obtained from equation (5) for $P_* = 10^{21.7}$ W Hz^{-1} sr^{-1}, $\beta = 1.4$, $C = 0.425 \times 10^{-4}$ and $\sigma = 0.44$ (see text for details). Seyfert 1/2 galaxies are not represented due to their small number.

Saunders et al. (1990). Note that we also considered a Φ_{SP} of the form given by Dunlop & Peacock, even though we do not show its trend in Fig. 8, given the unrealistic overprediction of the number of sources for $P \lesssim 10^{23}$ W Hz^{-1} sr^{-1}.

We note that none of the models can accurately describe the data. The Dunlop & Peacock (1990) predictions for radio galaxies underestimate the number density of objects for $P \lesssim 10^{22.5}$ W Hz^{-1} sr^{-1}, while the Rowan-Robinson et al. (1993) model, though able to reproduce the departure of the observed LF from the power-law behaviour for $P \lesssim 10^{23}$ W Hz^{-1} sr^{-1}, over-predicts the number density of sources with faint luminosities.

With the aim of investigating this result in more detail, we have then divided radio sources according to their spectral classification, and evaluated the local LF for each population taken individually. As in the case for the whole sample, values for the different classes of objects are illustrated in Table 1. Fig. 9 shows the results for the

early-type (bottom panel), early and E + AGN (middle panel) and late-type + SB (top panel) galaxies. The dashed lines in the bottom and middle panels are given by equation (4), which considers only the local density of 'classical', AGN-fuelled, steep-spectrum radio sources. In this case the agreement with the data is very good down to powers $P \simeq 10^{20.5} \, \mathrm{W \, Hz^{-1} \, sr^{-1}}$, especially if one includes all the objects which show spectra typical of early-type galaxies, regardless the presence of AGN emission lines.

Late-type/SB galaxies do not show the same power-law trend for the LF as the 'classical' radio sources (top panel of Fig. 9). Their LF shows a break at about $P \simeq 10^{22} \, \mathrm{W \, Hz^{-1} \, sr^{-1}}$, beyond which the contribution of this class of objects becomes rapidly negligible. For luminosities fainter than $P \simeq 10^{22}$, however, we note that their spatial density is comparable to that of early/E + AGN-type galaxies. It follows that, for $P \simeq 10^{21.5}$, late-type galaxies and starbursts make for about half of the whole spectroscopic sample.

Note that the sharp break in luminosity explains why late-type radio-emitting sources are only found in the nearby Universe, as already noticed in Section 3. In fact, the majority of these objects are not bright enough to show radio fluxes $S \geq 1 \, \mathrm{mJy}$ beyond redshifts $z \simeq 0.1$, and therefore were not observed by the FIRST survey. This feature in the LF also provides an explanation for the flattening – obtained for $b_J \gtrsim 17.5$ – of the curves describing the number of sources (both in the case of the photometric and spectroscopic samples) per magnitude interval presented in Fig. 4. As already shown by their radio-to-optical ratios, late-type/SB galaxies are in fact faint in radio and, being actively forming stars, bright in the optical b_J band. The absence of this class of sources for $P \gtrsim 10^{22} \, \mathrm{W \, Hz^{-1} \, sr^{-1}}$, as shown by their LF, implies that they fall out of the spectroscopic (and photometric) sample for $z \gtrsim 0.1$ *only* because of their faint radio fluxes and not due to optical magnitudes fainter than the chosen threshold. These objects would obviously appear as optically faint at higher redshifts, but they never reach this stage since they first disappear from the flux-limited radio survey. It therefore follows that, for $b_J \gtrsim 17.5$, only members of the population of early-type and E + AGN galaxies are included in both the photometric and spectroscopic samples, which explains the flattening in Fig. 4.

Finally, note that the last data point at the bright end of the LF for late-type and SB galaxies rises up towards higher spatial densities than predicted. Closer investigation reveals that the two objects responsible for this measurement, even though classified as late-type galaxies on the basis of their line-emission ratios, show spectra where the relative importance of the [O II]–[O III] lines seems to point out to an 'intermediate' case where both AGN and star formation activity are present within the same galaxy. This could then lead to a radio signal dominated by non-thermal emission, bringing these sources into the class of E + AGN galaxies.

When it comes to a comparison between observed and predicted LF for the population of late-type galaxies and starbursts, one has that predictions from Dunlop & Peacock (1990) (not shown for the
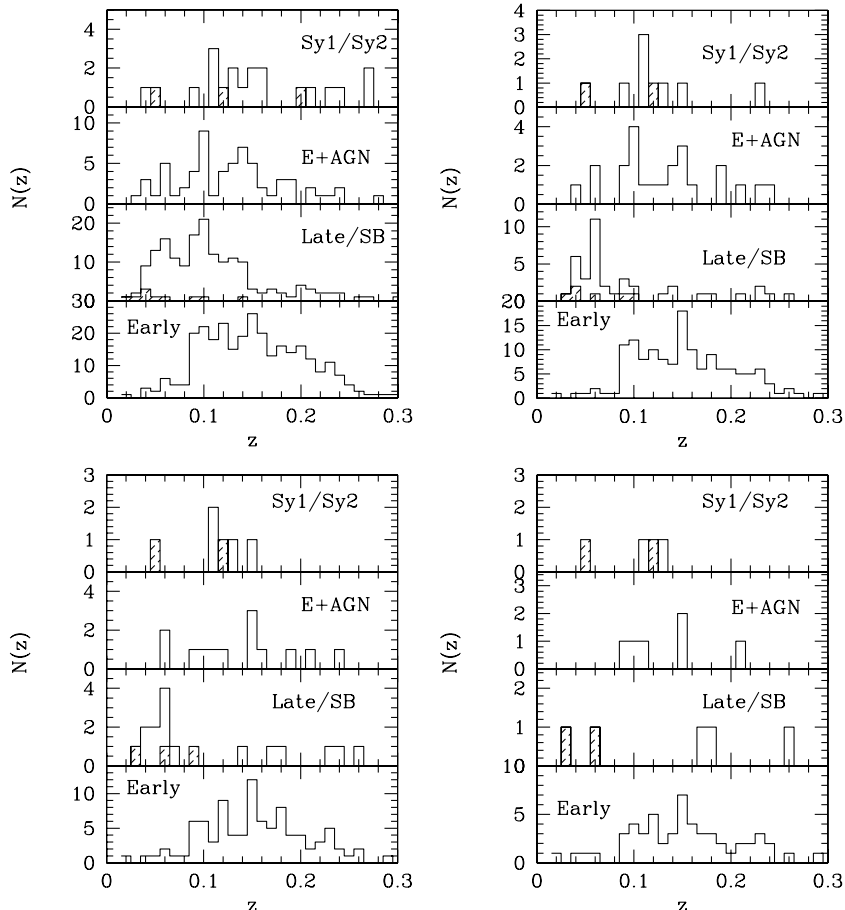
Figure 10. Redshift distributions for the different classes of sources in the spectroscopic sample: top left for $S \geq 1 \, \mathrm{mJy}$, top right for $S \geq 3 \, \mathrm{mJy}$, bottom left for $S \geq 5 \, \mathrm{mJy}$, and bottom right for $S \geq 10 \, \mathrm{mJy}$. In the Sy1/Sy2 panels, the shaded histograms represent the distribution of Seyfert 1 galaxies, while in the Late/SB panels, the shaded histograms are for the subclass of starburst galaxies.

reasons explained earlier in this section) agree with only the $P \simeq 10^{23}$ W Hz^{-1} sr^{-1} data point, grossly overestimating the contribution of this kind of sources at fainter luminosities. A better job is provided by the Rowan-Robinson et al. (1993) model, which can correctly reproduce both the broken power-law behaviour and the break luminosity. However, the slope of the faint-end portion of the predicted LF is too steep and, as previously noticed, this results in an overprediction of the number density of sources at these luminosities.

By using equation (5), we find that the best fit is obtained for $P_* = 10^{21.7}$ W Hz^{-1} sr^{-1}, $\beta = 1.4$, $C = 0.425 \times 10^{-4}$ and $\sigma = 0.44$ (long/short-dashed lines in Fig. 9), not far from the Rowan-Robinson et al. (1993) model, showing that late-type/SB galaxies have to be identified with those spirals and starbursts which dominate the counts at 60 μm. The above functional form can also, together with the LF given by Dunlop & Peacock (1990) for the population of ellipticals and represented by equation (4), correctly reproduce the total LF for radio sources in the 2dFGRS as illustrated by the long/short-dashed line in Fig. 8. The agreement, however, breaks down for $P \lesssim 10^{20.5}$ W Hz^{-1} sr^{-1}, due to the low space density of early- and E + AGN-type galaxies at such faint luminosities.

5   REDSHIFT DISTRIBUTION

Finally, we move on to the analysis of the redshift distribution of sources in the spectroscopic sample. Fig. 10 shows the results for different classes of objects and different flux cuts. In the top left panel we show the $S \geq 1$ mJy case, and in the top right panel the $S \geq 3$ mJy case, while the bottom left panel includes only those objects with $S \geq 5$ mJy, and the bottom right panel sources with $S \geq 10$ mJy.

The most striking feature in the various distributions is the drastic reduction of late-type galaxies for radio fluxes between 1 and 3 mJy. The tendency for these sources to be only present at ∼ 1 mJy level and fainter was already reported by, e.g., Windhorst et al. (1985), Danese et al. (1987) and Benn et al. (1993), even though their relative contribution to the total radio population was still an issue under debate. As already noted, one also sees that the distribution of late-type galaxies is very local, peaking at about $z \simeq 0.1$ and quickly fading off beyond redshifts $z \simeq 0.15$.

Early-type galaxies are instead more distant, starting to be the dominant population only for $z \gtrsim 0.1$. They also show a distribution which does not alter its shape for increasing limiting fluxes. E + AGN sources once again constitute an intermediate case between late- and early-type galaxies, and their number is drastically reduced only for fluxes $S \geq 5$ mJy.

As expected, Seyfert 2 galaxies all present low radio fluxes and are evenly distributed between $z = 0$ and $z = 0.3$. Of the three Seyfert 1s included in the spectroscopic sample within $z \leq 0.3$, only one has $S \leq 3$ mJy.

The combination of these trends for the different classes of objects gives rise to the *total* redshift distribution of $S \geq 1$ mJy radio sources within $z \leq 0.3$, although we note that the sample loses completeness beyond $z \simeq 0.2$. This distribution is presented in Fig. 11; as in Fig. 10, the flux limit in the panels increases clockwise from the top left panel between $S = 1$ and $S = 10$ mJy. The $z \simeq 0.05$ 'bump' shown by all the $N(z) - z$ histograms is principally due to late-type galaxies (with some contamination from E + AGN), while the maximum at $z \simeq 0.1$ which is present only in the $S \geq 1$ mJy plot, is due to superposition of late-type and early-type galaxies in that redshift range. For $S \geq 3$ mJy we see a rather sharp bimodal distribution, with a first maximum – principally due to very local star-forming galaxies which rapidly loses importance as one goes to higher flux cuts – and by a smooth increase in the number of sources with redshift between $z = 0.1$
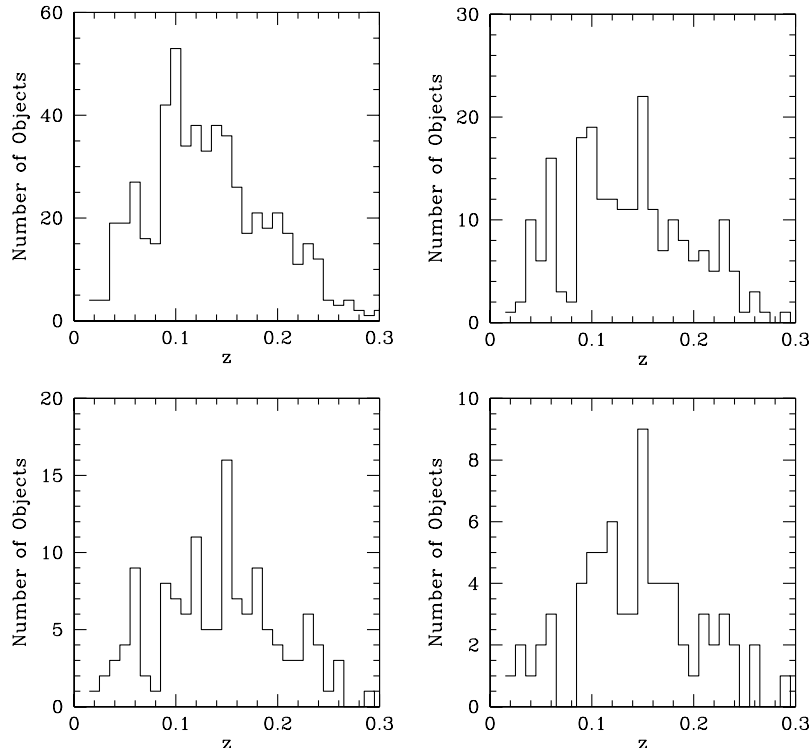
Figure 11. Redshift distributions for the whole spectroscopic sample up to $z = 0.3$: top left for $S \geq 1$ mJy, top right for $S \geq 3$ mJy, bottom left $S \geq 5$ mJy, and bottom right for $S \geq 10$ mJy.

Table 2. Spectral identifications.

Object	α (J2000)	δ (J2000)	Off	S1.4	bJ	R	z	Class	Emission Lines	Notes
266022	10 12 20.85	− 0 35 18.7	0.43	4.19	18.69	16.31	0.1865	Early	none	
266087	10 12 2.10	+0 52 51.8	1.30	1.08	18.89	17.71	0.1234	Late	Hα,S II,O III,Hβ,O II	
266263	10 11 7.55	− 0 2 32.1	0.65	1.69	16.02	?	0.0336	Late	Hα,S II,Hβ	O:Spiral
266264	10 11 4.84	− 2 2 35.5	0.76	4.10	19.06	16.48	0.1978	Early	none	
266279	10 11 0.13	− 2 18 29.8	1.08	1.17	15.81	15.55	0.0797	Early	none	
266343	10 10 42.91	− 1 47 18.6	1.55	3.08	16.09	14.66	0.0897	Early	O II,Hα	O:Merging
266383	10 10 30.56	− 1 54 18.5	1.00	4.61	16.85	16.00	0.0614	Late	Hα,S II,Hβ,O II	O:Irregular
266443	10 10 16.73	+0 19 24.2	1.16	2.60	19.13	18.31	0.1829	Late	Hα,O II,O III,Hβ	
266492	10 10 4.99	+1 53 3.8	1.02	3.13	17.70	16.72	0.0951	Early	none	
266557	10 9 51.57	+1 13 28.0	1.23	5.26	15.69	14.62	0.0459	Late	Hα,S II,Hβ,O II	
266582	10 9 42.27	− 0 32 41.4	1.77	1.49	18.01	16.96	0.0943	Early	none	
266612	10 9 35.72	+1 11 45.0	0.85	1.26	19.00	17.28	0.1863	Early	O II	
266637	10 9 27.55	− 1 27 2.4	0.78	9.18	18.74	?	0.1871	Early	none	
266888	10 8 20.75	+0 9 40.9	0.31	15.05	17.10	16.55	0.0933	Early	none	
266926	10 8 11.44	+0 29 59.5	1.37	336.1	17.33	16.09	0.0980	Early	none	R:Extended
266974	10 7 57.30	− 0 56 12.6	0.43	1.20	18.87	17.69	0.1548	Late	Hα,S II,O II,Hβ,O III	
267422	10 5 41.30	− 0 53 12.4	0.37	1.50	19.14	17.63	0.1500	Early	Hα	
267445	10 5 33.44	+0 17 59.2	1.53	8.44	18.67	16.73	0.2139	Early	none	
267455	10 5 27.15	− 0 52 28.8	0.97	1.03	19.02	17.02	0.2059	Early	none	
267466	10 5 23.57	+1 4 15.4	0.62	3.23	18.88	17.20	0.1765	Early	none	
267473	10 5 21.50	+0 5 18.6	0.31	8.04	19.12	17.26	0.1793	Early	none	
267508	10 5 12.29	+0 37 55.1	1.18	2.58	18.07	17.46	0.0630	Late	Hα,S II	
267540	10 5 2.75	− 0 42 33.4	1.28	3.67	18.62	16.84	0.1962	Early	none	
267567	10 4 52.00	− 1 50 12.6	0.60	12.59	17.63	16.26	0.1392	Early	O II	
267739	10 4 4.99	− 0 32 54.0	0.69	2.55	19.00	17.87	0.2889	Late	Hβ,O II,O III	
267861	10 3 27.10	− 1 32 46.5	1.04	11.45	15.84	15.01	0.0461	SB	Hα,S II,Hβ,O III,O II	O:Merging
267876	10 3 22.66	+0 50 25.6	1.86	16.05	17.65	?	0.0982	Early	none	
268002	10 2 41.78	− 1 20 9.2	0.04	8.33	18.98	16.91	0.1778	Early	none	
268035	10 2 32.52	− 0 29 43.0	0.88	1.98	17.34	16.60	0.0928	Late	Hα,S II,Hβ,O II	O:Irregular
268115	10 2 4.80	+1 33 55.6	1.19	1.33	18.71	17.61	0.0982	Early	Hα,S II	
268152	10 1 52.82	− 0 7 32.1	1.53	25.99	16.28	?	0.0333	Early	O II	
268552	10 0 5.27	+1 20 59.5	0.76	2.01	19.16	17.14	0.2199	Early	none	
268572	9 59 59.51	− 0 13 55.7	0.82	1.99	16.34	15.08	0.0904	Early	none	O:Merging
268631	9 59 39.05	− 1 14 53.2	0.30	11.12	17.52	15.96	0.1372	Early	O II	
268897	9 58 33.14	− 0 51 19.3	1.15	1.63	17.21	16.01	0.0858	E+AGN	O III,N II,Hα,S II,O II	
269141	9 57 21.15	+0 42 21.9	1.23	3.76	17.92	17.17	0.0873	SB	Hα,S II,Hβ,O III,O II	
269190	9 57 9.05	− 1 52 44.5	1.43	4.05	18.38	17.08	0.1215	Early	O II,Hα	
269199	9 57 9.25	+0 0 32.3	0.88	4.85	17.40	16.28	0.1254	Early	none	
269320	9 56 47.38	+1 15 23.4	0.58	1.97	17.71	16.36	0.0640	Early	Hα,S II	
269355	9 56 40.73	− 0 1 24.2	0.45	2.15	17.92	16.28	0.1395	Early	none	R:Core+lobes
269445	9 56 21.73	− 0 15 4.5	1.45	3.20	17.18	16.40	0.0210	SB	Hα,S II,Hβ,O II,O III	
269739	9 55 9.17	− 2 43 6.9	0.49	5.86	17.95	16.47	0.1633	Early	O II	
269805	9 54 50.18	− 1 44 19.7	0.55	1.62	17.63	16.89	0.1646	E+AGN	O III,O II,N II,Hβ	O:Irregular
270083	9 53 30.39	+0 26 54.5	0.26	12.77	16.48	15.09	0.0800	Early	none	
270188	9 52 56.96	− 0 47 30.6	1.18	16.88	17.29	?	0.0897	Early	none	O:Merging
270202	9 52 50.92	− 1 58 17.4	0.64	1.80	17.60	16.74	0.0564	Late	Hα,S II,Hβ,O II	
270236	9 52 40.11	+0 31 48.9	1.25	1.97	17.15	15.93	0.0779	Early	none	
270309	10 32 17.36	− 0 19 46.6	0.50	1.61	16.43	15.79	0.0558	Late	Hα,S II,O II	
270401	10 31 52.99	− 0 40 58.6	0.78	1.98	18.80	16.90	0.1496	Early	none	
270593	10 30 54.47	− 2 39 14.9	0.50	3.70	18.25	16.09	0.1337	Early	none	
270608	10 30 50.81	− 2 43 16.2	0.59	1.27	15.82	14.03	0.0297	E+AGN	N II,Hα,O III,S II,O II	O:Irregular
270646	10 30 41.24	+0 47 16.8	1.03	4.98	19.16	17.05	0.2177	Early	none	R:Double
270898	10 29 25.00	− 0 7 0.5	0.45	1.24	18.53	17.11	0.1183	Late	Hα,S II,O II	
271237	10 27 35.28	− 2 16 13.4	0.38	4.06	18.86	17.03	0.2179	Sy2	O III,O II,Hβ	
271337	10 27 9.07	+0 47 7.9	0.39	1.84	18.39	16.93	0.0901	Late	Hα,O II	
271402	10 26 54.63	− 0 32 30.1	0.20	2.78	15.88	14.81	0.0348	Late	Hα	
271484	10 26 35.18	− 0 1 58.7	0.77	1.41	18.49	17.26	0.1103	E+AGN	O III,Hα,N II,Hα,O II,Hβ	
271549	10 26 21.18	+0 41 5.2	0.82	5.98	15.76	14.28	0.0215	Late	Hα,S II,O III,Hβ	
271616	10 26 5.79	+0 34 12.3	0.20	2.09	17.18	15.35	0.0972	Early	none	
272058	10 24 7.27	− 2 3 46.0	1.95	8.20	15.64	?	0.0522	Early	none	O:Interaction
272077	10 24 1.48	+0 0 38.5	0.38	6.01	18.01	17.05	0.1265	Late	Hα,S II,O III,O II	
272224	10 23 31.99	+0 10 25.6	1.39	3.47	16.23	14.31	0.0958	Early	none	O:Interaction R:Double
272484	10 22 25.89	+0 12 54.4	0.84	5.68	19.26	17.22	0.2215	E+AGN	O II,O III	
272531	10 22 18.27	+0 30 50.3	0.70	167.37	17.68	15.82	0.0972	E+AGN	N II,S II,O III,O II	
272675	10 21 53.19	+2 12 39.7	0.47	1.29	16.56	14.95	0.0720	Early	none	
272740	10 21 32.74	+1 11 20.9	0.71	1.37	17.33	16.67	0.0941	Late	Hα,S II,Hβ,O II,O III	
272888	10 21 0.07	+0 7 50.1	0.41	5.15	18.25	16.26	0.1121	Early	none	
273382	10 19 17.50	+0 20 39.4	0.31	1.37	17.73	15.98	0.0206	Late	Hα,S II	
273708	10 18 6.67	+0 5 59.1	0.33	5.62	16.11	?	0.0485	E+AGN	N II,O III,Hα,S II,O II,Hβ	
273713	10 18 3.33	− 1 54 20.2	0.58	7.87	16.93	14.85	0.0609	Early	none	
273748	10 17 56.51	− 1 14 31.6	0.71	15.03	18.97	17.35	0.1625	Early	none	

Table 2 – *continued*

Object	α (J2000)	δ (J2000)	Off	S1.4	bJ	R	z	Class	Emission Lines	Notes
273837	10 17 40.57	− 0 28 54.9	0.60	1.57	16.18	14.39	0.0337	Early	none	
273855	10 17 36.76	− 2 25 4.2	0.71	1.31	17.49	15.62	0.0501	Early	Hα,N II,S II	
273860	10 17 38.19	− 0 27 12.0	1.14	1.62	16.77	?	0.0338	E+AGN	N II,Hα,S II,O III, O II	O:Spiral
273985	10 17 9.12	− 1 47 38.3	0.77	3.50	17.63	16.12	0.0455	Late	Hα, S II,Hβ,O II,O III	
274000	10 17 5.33	− 2 4 33.5	0.43	2.09	16.31	14.69	0.0625	E+AGN	N II,S II,O II, O III	
274107	10 16 40.60	+0 28 1.1	1.87	2.04	16.99	15.24	0.1225	Early	O II	
274137	10 16 29.31	− 0 53 49.6	0.62	1.02	17.56	16.04	0.0630	Late	Hα,S II,O II	
274176	10 16 19.34	− 1 35 52.2	0.45	2.82	18.60	15.89	0.2635	Early	none	
274379	10 15 36.22	+0 54 58.9	1.17	2.50	18.33	17.08	0.1205	Sy2	O III,Hα,S II,O II,Hβ	
274385	10 15 32.74	− 0 45 29.3	0.38	1.57	17.90	16.47	0.0626	E+AGN	O III,Hα,N II,S II,O II,Hβ	
274459	10 15 16.20	− 1 7 40.7	0.56	12.44	18.97	16.66	0.2015	Early	none	
274551	10 14 54.90	+0 33 37.3	0.79	2.60	17.37	16.14	0.1868	Sy1	Hα,O III,Hβ,Hγ,Hδ	O:Merging
274587	10 14 43.90	− 1 46 12.6	1.13	20.42	18.62	16.41	0.1986	E+AGN	O III,Hα,O II	
274690	10 14 23.58	− 0 4 40.6	0.88	5.49	19.33	16.97	0.2049	Early	none	
274734	10 14 16.08	+0 18 24.1	0.63	3.93	17.07	14.97	0.0955	Early	none	O:Merging
274829	10 13 55.30	− 1 51 9.2	1.39	1.00	16.57	15.33	0.0590	Late	Hα, S II,Hβ	O:Spiral
274895	10 13 44.86	− 0 7 13.5	1.26	2.23	16.47	16.00	0.0951	Early	none	
275115	10 12 59.14	− 1 50 46.0	0.35	6.23	19.06	16.70	0.2288	Late	O II,Hβ,O III	
275317	10 52 9.98	+0 53 32.9	0.68	2.64	17.43	16.22	0.1046	Early	none	
275322	10 52 8.11	+0 19 15.4	1.26	1.31	18.31	16.85	0.1075	Early	none	
275438	10 51 38.51	− 1 19 21.4	1.10	5.24	18.24	16.37	0.1081	E+AGN	O III,O II,Hα,N II,S II,Hβ	
275458	10 51 33.83	− 1 14 47.4	0.84	2.74	17.29	16.50	0.1077	Late	Hα,S II,Hβ,O II,O III	
275532	10 51 13.55	− 0 6 49.3	0.28	1.09	17.93	15.77	0.1480	Early	O II	
275616	10 50 51.82	− 0 54 12.6	1.36	1.03	17.04	16.60	0.0382	Late	Hα,S II,Hβ,O II	
275718	10 50 28.53	+0 28 7.2	0.97	4.93	18.91	18.10	0.2162	Late	O II,Hβ,O III	
275807	10 50 7.54	− 0 19 25.9	0.40	1.44	19.22	18.12	0.0749	Early	O II	
275988	10 49 30.86	− 0 36 35.4	1.15	1.01	18.18	16.74	0.0001	Star	none	
276002	10 49 26.56	+0 56 9.2	1.07	25.37	18.57	16.84	0.1049	Early	none	R:Double
276106	10 49 4.78	− 0 40 8.2	0.24	1.20	16.72	16.00	0.0383	Late	Hα,S II,Hβ,O II	
276139	10 48 54.82	− 0 50 44.3	1.16	1.78	19.00	17.00	0.2584	E+AGN	O III,O II	O:Spiral
276166	10 48 49.14	− 2 40 26.2	0.15	2.17	16.35	15.40	0.0369	Late	Hα,N II,S II,O III	O:Bulge+Disk
276184	10 48 45.59	− 0 0 31.0	0.71	1.48	18.28	16.33	0.1666	Early	none	
276317	10 48 13.91	− 0 8 51.2	1.28	1.20	18.65	17.33	0.0848	Late	Hα,Hβ,O II	
276367	10 48 1.89	− 1 30 15.2	0.99	5.13	17.80	16.69	0.1670	Early	O II	O:Interaction
276625	10 46 57.28	+0 53 33.9	0.64	1.75	18.24	17.11	0.1510	E+AGN	N II,O III,O II	
276745	10 46 33.10	− 2 17 13.9	0.90	9.91	18.95	16.49	0.1669	Early	none	
276769	10 46 29.16	+0 20 4.6	0.45	1.24	18.19	17.12	0.0497	Late	Hα,S II,Hβ,O III	
276835	10 46 15.50	− 1 43 13.8	0.61	2.65	15.85	15.17	0.0531	Late	Hα,S II,Hβ	O:Irregular
276897	10 46 2.28	+0 47 0.4	0.89	1.09	18.34	15.88	0.1628	Early	none	
276947	10 45 50.19	+0 27 34.3	0.65	3.40	17.04	15.49	0.0768	Early	none	
277016	10 45 33.31	− 1 37 22.2	1.06	1.13	18.97	17.62	0.2265	Early	O II	
277059	10 45 23.82	− 1 15 44.0	0.39	4.08	16.52	15.64	0.0392	Sy2	O III,Hα,N II,S II,Hβ,O II	
277118	10 45 9.50	+1 32 53.0	0.68	1.02	17.73	15.86	0.1187	Early	none	
277122	10 45 6.81	− 0 27 47.9	0.84	1.08	18.36	17.49	0.1603	Late	Hα,Hβ,O II,O III,S II	
277137	10 45 3.59	+0 26 2.1	1.08	3.02	15.63	14.48	0.0263	Late	Hα,S II,O III,O II	O:Merging
277151	10 45 0.40	− 0 15 54.4	0.30	4.17	18.25	?	0.0918	Sy2	O III,Hα,S II,Hβ,O II	
277175	10 44 56.47	− 0 20 50.5	0.34	3.47	18.78	17.45	0.1930	Late	Hα,O II,Hβ,O III	
277234	10 44 43.40	+1 42 40.5	1.24	1.43	18.24	16.90	0.1120	E+AGN	N II,O III,Hα,S II,O II	
277713	10 43 15.97	+0 50 59.4	0.37	1.30	18.17	?	0.1234	Early	none	
277721	10 43 14.50	− 1 5 15.5	0.81	1.37	16.93	?	0.0383	Late	Hα,S II,Hβ	
277761	10 43 7.18	− 1 29 39.7	0.84	1.70	17.56	15.68	0.0946	Early	none	
278013	10 42 24.13	− 0 8 17.0	0.99	2.27	17.66	?	0.1381	Early	none	
278059	10 42 18.52	+0 8 19.6	0.87	1.44	18.44	16.49	0.1247	E+AGN	Hα,S II,O III,O II	
278326	10 41 29.06	− 0 38 1.3	0.61	47.49	18.00	15.69	0.1360	Early	none	R:Double
278490	10 40 59.63	− 0 34 48.4	1.30	9.94	17.56	15.11	0.1368	Early	none	
278711	10 40 7.07	+0 26 34.7	0.36	1.87	18.15	16.24	0.1322	Early	none	
278870	10 39 32.78	− 0 34 19.5	1.52	1.31	19.08	17.66	0.2276	E+AGN	O III,O II,Hβ	
278965	10 39 15.66	− 0 39 17.6	0.28	30.92	17.53	16.72	0.0771	E+AGN	Hα,N II,O III,S II,O II,Hβ	
279222	10 38 25.07	− 0 23 34.0	0.63	34.06	16.76	15.45	0.0962	Sy2	O III,Hα,O II,S II,Hβ	
279272	10 38 13.33	− 1 22 28.3	0.15	1.75	17.53	16.65	0.0874	Late	Hα,O III,S II,Hβ,O II	O:Irregular
279337	10 37 58.71	− 0 5 46.4	0.33	1.12	18.97	17.43	0.2230	Late	O II,O III,Hβ	
279493	10 37 15.75	+0 4 48.6	1.38	1.16	16.57	16.45	0.0823	Late	Hα,N II,Hβ,S II,O II	
279526	10 37 5.71	− 0 42 32.2	1.14	3.35	18.74	17.42	0.0821	E+AGN	N II,Hα,S II,O II	
279820	10 35 49.42	− 0 14 20.9	0.99	2.23	17.21	16.50	0.0280	SB	Hα,S II,Hβ,O III,O II	
280061	10 34 38.21	− 0 51 10.6	0.64	3.07	16.93	16.71	0.0735	Late	Hα,S II,Hβ,O II	
280076	10 34 31.31	− 2 15 41.7	1.68	2.24	19.38	17.50	0.2219	Sy2	O III,O II,Hβ	
280200	10 34 7.86	− 1 12 26.5	1.20	1.34	19.02	17.52	0.2050	Late	O III,Hα,O II,Hβ	O:Irregular
280411	10 33 21.70	+0 6 1.3	1.32	1.18	19.05	17.95	0.1868	Late	Hα,O II,Hβ,O III	
280423	10 33 19.75	− 0 36 6.0	0.63	1.72	16.45	15.02	0.0507	Late	Hα,S II,O II	O:Spiral?
280490	10 33 0.63	− 0 22 49.9	1.10	1.31	17.26	16.11	0.0549	Late	Hα,S II,O II	
280529	10 32 52.91	− 0 44 36.3	1.08	2.55	17.36	16.19	0.0857	Late	Hα,Hβ,O II,O III	

Table 2 – *continued*

Object	α (J2000)	δ (J2000)	Off	S1.4	bJ	R	z	Class	Emission Lines	Notes
281483	11 5 39.01	+2 2 57.2	0.58	212.83	17.98	16.80	0.1066	Sy1	Hα,Hβ,Hγ,Hδ	R:Extended
281522	11 5 20.70	+0 53 16.3	1.41	1.69	17.31	16.22	0.0963	Early	O II	
281682	11 3 51.17	+0 52 48.3	1.06	1.51	18.76	17.37	0.1661	Early	none	
281746	11 3 13.15	+1 8 27.3	0.97	1.55	18.73	17.76	0.1112	Late	Hα,S II,Hβ,O II	
281802	11 2 17.20	+0 57 59.6	1.10	1.91	18.16	17.53	0.1023	Late	Hα,S II,O II,O III,Hβ	
282062	10 58 26.56	+0 34 30.0	0.33	2.90	19.10	18.18	0.0852	Early	Hα,S II	
282487	11 12 28.03	− 1 12 23.5	1.26	4.34	19.37	17.29	0.2548	Early	none	
282488	11 12 27.30	− 1 22 44.7	0.48	1.16	18.54	17.57	0.1911	Early	Hα	
282493	11 12 22.18	− 0 15 19.7	0.50	2.38	17.59	16.76	0.1238	E+AGN	Hα,N II,O III,S II,O II,Hβ	
282608	11 11 0.64	− 0 53 34.6	0.94	7.70	16.78	16.06	0.0909	Sy2	O III,Hα,N II,S II,O II,Hβ	O:Merging
282706	11 10 13.15	− 0 34 25.1	0.25	2.65	18.06	17.08	0.0395	Late	Hα,S II,O II	
282925	11 8 27.46	+0 14 54.9	0.58	1.83	18.35	17.57	0.1269	Late	Hα,S II,O III,Hβ,O II	
283081	11 6 57.84	− 1 5 49.7	0.38	1.36	18.82	17.55	0.0894	Late	Hα,O II	
283088	11 6 51.16	− 0 59 56.8	0.58	84.54	17.46	16.00	0.1132	Early	none	
283180	11 5 54.17	− 0 9 50.5	0.45	5.38	19.36	17.55	0.1557	Early	O II	
283309	11 3 50.10	− 0 36 6.6	0.39	4.71	17.05	15.76	0.0838	Early	none	
283414	11 2 37.36	− 1 6 43.2	0.94	1.37	18.91	17.21	0.1555	Early	O II	
283426	11 2 30.92	− 1 6 18.4	0.21	59.87	18.88	17.25	0.1567	Early	Hα,O II	
283607	11 0 19.98	− 0 59 29.0	0.23	1.37	18.18	16.72	0.1027	Early	none	
283640	10 59 28.88	− 1 1 39.5	0.48	1.72	18.32	?	0.1860	Early	none	
283666	10 59 2.61	+0 7 18.5	0.23	1.31	17.96	16.47	0.1096	Early	none	
283727	10 58 11.40	+0 9 56.6	1.29	1.56	17.37	16.97	0.0801	Late	Hα,Hβ,O II,S II	
283760	10 57 40.69	− 1 9 54.2	0.91	1.77	18.19	16.62	0.1083	E+AGN	O III,Hα,N II,S II,O II,Hβ	
283853	10 56 21.58	− 0 53 21.3	0.17	2.13	17.18	16.55	0.0755	Late	Hα,O III,Hβ,S II,O II	
284063	10 53 40.41	+0 9 3.1	0.75	11.53	17.39	15.70	0.1082	Early	none	
284254	11 11 11.47	− 1 50 50.2	0.52	25.37	18.38	16.45	0.1951	Early	none	R:Double
284424	11 9 8.17	− 1 35 22.7	0.31	1.91	19.38	18.17	0.1972	Late	Hα,O II,O III,Hβ	
284434	11 8 58.43	− 1 49 32.8	1.37	62.16	17.96	?	0.1060	Early	none	
284560	11 7 17.58	− 1 57 4.8	1.28	1.40	16.65	16.12	0.0672	Late	Hα,O III,O II,Hβ	O:Spiral?
284757	11 4 53.65	− 1 36 23.9	1.00	6.72	16.94	15.47	0.1009	Early	none	
285054	10 58 35.36	− 2 35 53.1	0.60	210.17	16.45	15.64	0.0362	Sy1	N II,Hα,S II,O III,Hβ,O II	
285068	10 58 17.49	− 1 47 47.5	0.48	2.69	18.35	17.22	0.1316	E+AGN	O III,Hα,N II,Hβ,O II	
285152	10 57 6.44	− 2 13 0.9	0.71	2.27	18.43	16.00	0.1863	Early	none	
285226	10 55 53.37	− 2 10 42.5	0.50	3.16	18.19	16.68	0.0929	Early	O II	
285354	10 52 53.75	− 1 53 15.5	1.10	3.34	16.58	15.60	0.0259	Late	Hα,N II,Hβ	
285362	10 52 39.11	− 1 41 42.9	0.88	6.96	19.43	17.12	0.2311	Early	none	
285379	11 32 29.92	− 0 32 39.1	0.28	2.73	18.85	17.36	0.1324	Early	none	
285397	11 32 23.12	+0 52 18.0	0.72	19.22	19.34	16.71	0.1972	Early	none	R:Extended
285456	11 32 6.65	− 0 44 44.1	0.37	1.84	18.67	17.95	0.1043	Late	Hα,N II,Hβ,S II,O III,O II	
285716	11 30 55.35	− 1 24 7.8	1.09	1.41	18.16	17.60	0.0732	Late	Hα,S II,O III	
285731	11 30 53.44	+0 52 51.4	0.14	2.22	18.65	17.33	0.1271	Early	N II,O II	
285732	11 30 52.64	− 1 29 39.7	0.96	1.95	16.53	16.80	0.0728	Late	Hα,N II,O II,Hβ,S II,O III	O:Irregular
285896	11 30 10.48	− 1 26 51.6	1.34	63.03	17.34	16.57	0.1195	Early	Hα,O II	
285914	11 30 6.90	− 0 7 16.1	0.83	2.68	18.44	17.98	0.1151	Late	Hα,N II,O II,S II	O:Interaction
285923	11 30 4.15	− 1 2 58.1	0.41	2.27	17.57	?	0.1218	Early	none	
286105	11 29 17.99	− 1 42 29.2	0.80	5.22	15.74	15.29	0.0431	Late	Hα,S II,Hβ	
286428	11 27 54.35	− 1 13 31.9	0.21	1.60	15.75	14.87	0.0424	Early	Hα	
286543	11 27 27.61	− 2 32 50.2	0.40	24.39	18.42	16.74	0.1443	Early	O II	
286670	11 26 55.63	+0 40 47.1	0.76	2.15	17.83	17.60	0.0903	Late	Hα,S II,Hβ,O III,O II	O:Merging
286732	11 26 40.67	− 1 41 38.2	1.06	8.38	16.25	16.00	0.0462	E+AGN	O III,Hα,N II,S II,O II,Hβ	
286874	11 26 6.90	− 1 59 14.7	0.71	1.29	18.59	17.23	0.1195	Early	none	
286921	11 25 56.97	− 0 5 3.1	0.92	1.76	17.96	16.81	0.1049	Early	none	
286927	11 25 54.75	− 1 35 2.0	0.40	1.42	17.31	16.66	0.0456	Late	Hα,S II,O III,Hβ,O II	
286950	11 25 50.29	− 2 28 8.4	1.33	1.29	17.87	17.30	0.1196	E+AGN	O III,Hα,N II,S II	
287242	11 24 27.13	− 2 42 58.7	0.29	3.16	18.01	16.38	0.1427	Early	none	
287249	11 24 26.12	− 0 25 38.0	0.32	1.21	17.70	17.19	0.0485	E+AGN	O III,Hα,N II,S II,O II	
287298	11 24 14.61	+0 58 36.9	0.28	1.66	18.98	17.85	0.1005	Early	none	
287312	11 24 8.62	− 1 9 28.7	0.55	4.95	15.70	?	0.0294	E+AGN	O III,Hα,N II,S II,O II,Hβ	O:Bulge+Disk
287361	11 23 58.96	− 0 0 24.9	0.47	1.14	17.93	17.47	0.0645	Early	Hα,N II,S II	O:Spiral
287369	11 23 56.00	− 2 42 20.4	1.13	1.93	17.00	?	0.1163	Late	Hα,N II,O III,Hβ,S II,O II	
287418	11 23 45.60	− 1 16 28.4	0.73	3.67	16.99	16.38	0.0765	E+AGN	Hα,N II,O III,O II	O:Spiral
287446	11 23 35.16	− 1 33 56.3	0.85	10.02	15.51	14.71	0.0444	Late	Hα,S II,Hβ,O II,O III	
287596	11 23 7.73	− 0 32 37.8	0.89	2.58	18.99	17.17	0.1937	Early	none	
287782	11 22 39.15	+0 43 12.8	0.89	1.54	16.66	16.37	0.0724	Late	Hα,N II,Hβ,S II,O II,O III	
287791	11 22 36.85	+0 29 33.6	0.54	6.21	17.53	16.48	0.1035	Early	none	
287903	11 22 17.78	− 1 52 59.1	0.89	2.19	18.06	17.83	0.1084	Late	Hα,S II,Hβ,O II,O III	
287982	11 22 2.73	− 1 35 55.6	0.67	2.20	18.68	16.94	0.1539	Early	none	
288022	11 21 54.52	+0 33 43.7	1.37	1.96	17.12	?	0.0709	Late/E+AGN	Hα,O III,O II	
288105	11 21 32.33	− 1 40 47.7	0.10	5.93	18.32	16.46	0.1435	Early	none	
288217	11 21 11.51	− 0 17 38.7	0.26	1.05	17.31	16.46	0.0978	Early	N II,S II	
288228	11 21 9.53	+0 12 41.7	1.50	15.49	17.59	16.33	0.1039	Early	none	

Table 2 – *continued*

Object	α (J2000)	δ (J2000)	Off	S1.4	bJ	R	z	Class	Emission Lines	Notes
288277	11 20 59.70	+0 32 3.5	1.12	3.15	15.39	14.37	0.0243	Late	Hα,S II,Hβ,O II,O III	
288345	11 20 45.18	−0 8 54.5	0.89	1.29	17.62	17.27	0.0252	Early	O II	
288465	11 20 17.61	+0 24 21.0	1.28	2.26	18.99	17.99	0.2049	Early	O II	
288666	11 19 29.66	−0 44 30.9	0.66	1.94	17.21	16.98	0.0734	Early	Hα,N II	
288813	11 18 57.47	−1 11 30.4	1.76	1.33	18.09	17.48	0.0652	Late	Hα,N II,O III,Hβ,O II	
289044	11 18 7.45	+0 27 34.5	0.68	6.63	18.47	17.07	0.1670	Early	O II	
289103	11 17 54.66	−1 56 47.5	0.40	4.53	14.75	13.41	0.0417	Late	Hα,N II,O II	
289200	11 17 32.87	−0 11 16.1	1.03	5.10	15.99	14.89	0.0397	Late	Hα,N II,S II,O II	
289621	11 15 53.83	+0 47 33.6	1.69	1.89	18.13	17.94	0.1407	Late	Hα,N II,O III,O II	
289628	11 15 52.00	−0 4 38.4	1.47	9.26	16.80	16.52	0.0391	Late	Hα,N II,S II,O III,O II	
289644	11 15 46.93	−2 35 51.7	1.30	1.67	18.17	17.55	0.1340	Early	Hα,N II	
289694	11 15 38.21	+0 29 40.7	1.01	1.62	18.87	17.73	0.1133	E+AGN	Hα,N II,S II	
289785	11 15 19.10	+0 23 7.4	0.25	3.46	18.03	16.42	0.1436	Early	none	
289793	11 15 17.45	+0 7 43.3	0.54	1.90	18.61	17.37	0.1133	Early	O II	
290547	11 52 19.57	−2 23 16.5	1.00	2.76	18.60	17.17	0.1644	Early	none	
290719	11 51 31.44	−0 3 3.9	0.47	2.41	16.54	16.65	0.0469	E+AGN	N II,O III,Hα,S II,Hβ,O II	
291061	11 49 47.82	+0 7 42.3	0.64	2.48	18.78	17.94	0.0767	Early	none	
291091	11 49 38.61	−0 21 10.6	0.12	2.89	17.73	17.25	0.0847	E+AGN	N II,Hα	
291127	11 49 30.12	−1 5 11.8	0.46	1.55	15.31	?	0.0192	E+AGN	N II,O III,S II,O II	
291142	11 49 26.11	−0 18 19.0	0.92	2.32	17.38	16.19	0.0833	Early	none	
291220	11 49 7.98	−0 57 5.1	0.70	1.89	19.15	17.56	0.2647	E+AGN	O II,O III	
291655	11 47 21.00	−1 42 12.2	1.70	4.15	17.24	?	0.0921	Early	none	
291786	11 46 49.45	−1 28 57.2	1.13	1.06	19.14	17.98	0.1561	Early	Hα	
291873	11 46 24.98	−1 45 13.7	0.78	2.78	19.11	17.87	0.1645	Early	O II	
291953	11 46 6.97	−1 5 38.1	1.62	3.67	18.17	16.83	0.1159	Early	none	R:Double
292291	11 44 48.36	−1 9 31.4	0.62	17.98	17.90	17.16	0.0778	Early	Hα,O II	
292329	11 44 38.30	−2 1 1.9	0.89	1.42	19.11	17.86	0.1318	E+AGN	N IIHα,O III,O II	
292380	11 44 25.99	−1 57 26.3	0.24	3.62	16.76	15.76	0.0763	Early	none	
292449	11 44 4.78	−2 2 27.7	0.67	1.71	17.81	17.87	0.0677	Late	Hα,S II,Hβ,O III,O II	
292538	11 43 42.98	−2 14 6.9	0.59	2.10	18.07	18.33	0.1206	SB	Hα,O III,Hβ,O II,S II	
292550	11 43 41.08	−0 11 51.8	0.46	1.49	19.22	17.99	0.1503	Late	Hα,N II,S II,O II	
292553	11 43 40.08	−1 26 28.3	0.73	1.25	18.57	17.93	0.1235	Early	Hα	
292557	11 43 38.90	−1 38 49.8	0.57	4.25	17.25	16.79	0.0431	Late	Hα,S II,Hβ	
292806	11 42 30.93	−2 15 5.8	0.38	7.68	16.04	15.13	0.0477	Early	none	
292858	11 42 12.30	+0 20 1.4	1.59	24.98	15.34	14.72	0.0168	SB	Hα,O III,Hβ,S II,O II	O:Merging
292879	11 42 3.40	+0 51 34.9	0.72	17.68	18.92	18.46	0.2450	Late	O II,Hβ,O III	
292934	11 41 46.70	−0 31 5.7	0.46	1.83	17.18	?	0.1061	Early	none	
292942	11 41 44.64	−0 41 17.5	0.24	3.33	17.66	17.35	0.0501	Late	Hα,S II,Hβ,O II,O III	
292990	11 41 26.56	−2 34 5.4	0.59	43.47	19.21	18.82	0.1601	Late	Hα,S II,O II,Hβ,O III	
293157	11 40 39.06	−0 18 22.1	0.99	1.62	17.44	17.79	0.1122	Late	Hα,S II,Hβ,O II	O:Merging
293288	11 40 6.84	−0 27 57.7	0.35	2.68	18.84	17.92	0.0749	Early	N II,Hα,O III	
293372	11 39 42.86	−2 39 46.8	1.20	1.29	19.28	17.63	0.2896	Early	O II	
293458	11 39 15.01	−2 41 9.5	2.00	2.04	17.17	16.84	0.1033	E+AGN	Hα,N II,O III,S II	R:Double
293482	11 39 5.57	−2 37 28.7	1.50	3.16	18.35	17.14	0.1692	Early	none	R:Double
293507	11 38 58.50	−0 16 30.7	0.70	1.60	18.14	18.00	0.1637	E+AGN	Hα,N II,O III,S II,Hβ,S II,O II	
293791	11 37 24.52	−2 5 51.6	0.83	3.13	17.43	17.13	0.0786	Late	Hα,Hβ,S II,O II	
294053	11 35 51.38	+2 5 28.6	0.86	1.28	18.37	17.76	0.0748	Late	Hα,S II,Hβ,O II	
294355	11 34 19.76	−2 2 25.8	0.49	4.70	18.47	17.79	0.1123	E+AGN	Hα,N II,S II,O III,O II	
294356	11 34 20.50	+0 18 56.3	1.13	1.28	17.01	16.47	0.0293	Late/E+AGN	Hα,N II,S II,O III,O II	
294391	11 34 9.26	−1 35 42.7	1.30	2.52	15.79	15.12	0.0227	Late	Hα,S II,Hβ	
294492	11 33 34.69	−2 16 48.8	0.42	8.22	15.74	15.06	0.0405	Late	Hα,S II,Hβ,O II,O III	
294617	11 32 58.75	+0 55 27.9	0.40	2.97	18.12	16.64	0.1212	Early	none	
294674	11 32 43.25	−2 11 59.7	0.24	3.98	16.39	15.53	0.0420	Late	Hα,Hβ,S II,O II	
294700	11 32 36.61	−2 17 5.6	0.82	1.87	17.49	16.08	0.0499	Late	Hα,S II,Hβ,O II,O III	
295046	12 8 4.42	+0 33 53.2	0.51	1.64	17.51	17.73	0.0953	Late	Hα,Hβ,S II,O II	
295141	12 6 52.47	+0 58 22.7	0.30	1.98	18.54	16.96	0.1120	Early	none	
295697	12 1 3.36	+1 0 11.6	0.48	2.03	17.71	18.11	0.0853	Late	Hα,Hβ,S II,O II,O III	
295908	11 58 44.57	+0 49 34.3	0.07	2.58	18.89	17.22	0.2017	Early	none	
295959	11 58 17.27	+0 46 2.1	0.53	2.05	17.24	?	0.0781	Late	Hα,Hβ,O III,O II	
296043	11 57 19.04	+0 48 8.7	0.86	1.20	18.59	17.70	0.1235	Early	Hα,O II	
296045	11 57 23.05	+0 29 13.3	1.44	2.40	16.56	17.01	0.0470	Late	Hα,S II,Hβ,O II	O:Spiral?
296078	11 56 57.00	+1 6 57.1	0.64	3.27	16.61	16.81	0.0392	Late	Hα,S II,Hβ,O II	
296396	12 12 4.56	−0 39 14.2	0.92	1.09	17.46	17.05	0.0723	E+AGN	Hα,N II,O III,S II,O II,Hβ	
296397	12 12 6.89	−1 4 22.2	1.90	2.86	17.94	18.12	0.1144	Late	Hα,O II,Hβ,S II,O III	
296549	12 10 6.00	+0 26 39.3	0.47	3.93	18.01	17.49	0.1278	Late	Hα,S II,Hβ,O II	
296614	12 9 25.22	−0 57 51.5	0.15	9.03	19.00	17.57	0.1301	Early	O II	
296680	12 8 23.87	−0 57 17.3	0.13	1.20	19.27	?	0.1792	Early	none	R:Double
296886	12 5 41.39	−0 14 20.3	1.10	1.61	18.73	17.43	0.1765	E+AGN	Hα,N II,S II,O III,O II	O:Irregular
296904	12 5 26.88	+0 17 44.7	0.35	3.06	17.98	16.66	0.1301	Early	none	
297089	12 3 4.34	−0 7 28.2	1.45	3.64	17.62	17.66	0.1219	E+AGN	N II,Hα,O III,O II	O:Merging
297124	12 2 42.38	−1 23 46.2	0.73	58.18	19.40	16.65	0.2482	Early	none	R:Double

Table 2 – *continued*

Object	α (J2000)	δ (J2000)	Off	S1.4	bJ	R	z	Class	Emission Lines	Notes
297219	12 1 34.44	+0 20 50.3	1.20	1.52	17.19	17.66	0.0384	Late	Hα,S II,Hβ,O II	
297252	12 1 10.35	−0 10 11.3	1.42	1.57	18.95	18.47	0.1808	Late	Hα,O II,O III,Hβ	
297259	12 1 6.19	−0 7 1.6	0.71	62.64	18.62	16.76	0.1650	Early	none	
297313	12 0 37.70	+0 1 25.5	0.61	1.08	18.46	17.43	0.0950	Early	none	
297315	12 0 36.04	−0 31 37.2	0.10	2.90	17.14	17.25	0.0831	Late	Hα,Hβ,O II	
297358	12 0 15.06	+0 7 35.4	0.60	1.03	18.99	16.66	0.1784	Early	none	
297398	11 59 56.07	−0 19 23.4	0.45	5.03	17.28	?	0.0832	Early	none	
297428	11 59 41.62	−0 31 54.5	1.32	2.80	18.59	?	0.1781	Early	none	R:Core+lobes
297478	11 59 9.71	+0 0 6.3	0.41	1.45	16.76	16.94	0.0464	Late/E+AGN	N II,Hα,O III,S II,Hβ,O II	
297573	11 58 24.78	−0 4 26.3	0.67	2.76	17.62	16.20	0.1068	Early	none	
297645	11 57 56.82	+0 12 21.2	0.22	3.32	17.94	16.82	0.1081	Early	none	
297746	11 57 7.23	−0 48 8.7	1.75	1.64	18.28	18.25	0.1262	Late	Hα,Hβ,S II,O II	
297747	11 57 6.37	−0 58 38.4	0.11	5.25	16.85	16.14	0.0770	Early	none	
297825	11 56 20.01	−0 12 20.2	1.29	2.14	16.20	16.34	0.1073	Early	none	
297919	11 55 38.05	−0 46 14.9	0.84	2.78	16.42	?	0.0647	Late	Hα,N II,O III,Hβ,S II,O II	O:Spiral
297923	11 55 36.05	−1 24 5.0	1.26	1.47	17.45	17.53	0.0765	Late	Hα,N II,S II,Hβ,O II	O:Bulge+Disk
297929	11 55 34.41	−1 14 17.2	0.45	15.70	17.75	?	0.1272	Early	none	
297936	11 55 30.64	−1 15 41.3	0.73	1.78	15.85	15.92	0.0192	Late	Hα,N II,S II,Hβ	O:Spiral?
297953	11 55 19.66	−1 24 32.2	0.34	2.82	19.13	18.19	0.1446	Sy2	O III,Hα,N II,O II,S II	
297984	11 55 0.51	−1 25 52.5	1.33	112.61	18.29	16.83	0.1632	Early	none	R:Double
298044	11 54 12.30	+0 8 11.8	0.62	1.70	14.43	?	0.0038	SB	Hα,Hβ,O III,S II,O II	
298099	11 53 27.42	−1 10 52.3	0.12	3.17	16.99	17.08	0.0803	Late	Hα,Hβ,O II,S II,O III	O:Spiral
298218	12 11 49.92	−2 14 0.0	0.55	3.33	17.76	16.66	0.0790	Early	none	
298227	12 11 38.98	−1 29 44.5	0.59	4.89	19.26	17.35	0.2018	Early	none	R:Double?
298320	12 9 43.64	−2 5 0.0	1.10	23.71	17.61	16.65	0.1000	Early	none	R:Jets?
298359	12 9 9.67	−2 2 8.3	0.26	1.30	18.97	16.99	0.1756	Early	none	
298444	12 7 18.63	−1 39 31.3	0.86	8.16	18.75	?	0.1816	Early	none	R:Double
298445	12 7 18.73	−1 47 57.0	0.49	1.41	17.97	17.83	0.1074	Late	Hα,S II,Hβ,O II	
298579	12 3 57.26	−1 38 27.3	0.91	2.22	17.84	17.94	0.0985	Late	Hα,Hβ,S II,O III,O II	
298619	12 3 8.48	−1 59 56.8	1.31	6.93	17.67	16.31	0.1310	Early	none	
298629	12 3 3.57	−1 55 50.7	0.99	1.36	19.12	17.18	0.1534	Early	none	
298664	12 2 26.66	−1 29 15.9	1.99	12.40	17.83	17.98	0.1511	Late	Hα,O II,O III,S II	
298694	12 1 49.73	−1 53 28.3	0.79	2.65	17.27	17.75	0.0907	Late	Hα,O III,Hβ,S II,O II	O:Merging
298774	12 0 6.04	−2 26 34.9	0.37	2.98	17.28	17.18	0.1028	Early	Hα,O II	
298857	11 58 45.42	−1 48 22.8	1.40	3.71	17.94	17.69	0.0880	Late/E+AGN	Hα,N II,O III,S II,O II,Hβ	
298887	11 58 20.58	−2 9 47.3	0.46	2.25	17.66	?	0.0827	Early	O II	
299070	11 54 59.88	−2 2 13.9	0.42	1.15	17.54	17.38	0.0773	Early	Hα	
299146	11 53 52.84	−1 37 39.4	1.58	26.57	19.18	17.16	0.2782	Early	none	R:Extended
299186	11 53 30.95	−1 44 4.6	0.70	82.90	17.25	?	0.1360	Early	none	
299339	12 31 23.28	+0 32 11.3	1.71	2.34	17.90	?	0.0619	Late	Hα,S II	
299536	12 28 13.69	+0 37 0.1	0.49	2.02	17.76	17.72	0.1080	Late	Hα,Hβ,O II,S II,O III	
300599	12 32 22.22	+0 0 41.4	0.31	4.09	16.39	16.66	0.0437	Late	Hα,S II,O III,O II,Hβ	
300657	12 31 38.03	−0 9 8.3	0.99	1.28	17.29	16.67	0.0796	Early	none	
300777	12 29 58.88	+0 1 37.5	0.70	2.16	16.81	16.47	0.0076	Late	Hα,S II,Hβ,O III	
300922	12 27 59.99	−0 49 15.1	0.31	9.85	18.42	17.33	0.1571	Early	O II	
301004	12 26 58.15	+0 25 14.8	1.15	4.33	18.19	17.47	0.1194	Early	Hα,O II	
301006	12 26 56.69	−0 4 16.9	0.67	1.01	19.36	18.42	0.1609	Early	O II	
301193	12 23 14.49	−0 15 22.7	1.78	17.52	18.53	17.62	0.1569	Early	O II	R:Double
301231	12 22 39.24	−0 58 50.9	1.83	1.80	17.97	17.18	0.1753	Early	O II	
301285	12 21 32.43	+0 12 56.4	1.57	2.67	17.03	15.93	0.1731	Early	none	O:Merging
301387	12 20 12.56	−1 5 32.9	0.90	1.97	18.98	18.30	0.1181	Sy2	O III,Hα,N II,S II,O II,Hβ	
301410	12 19 46.60	−1 12 1.1	0.84	1.17	17.65	17.79	0.0849	Late	Hα,Hβ,O III,O II,S II	
301577	12 17 30.77	+0 23 57.3	1.98	32.18	18.46	17.64	0.0014	Early	O II	R:Core+lobes?
301626	12 17 4.74	−0 55 9.1	0.96	3.28	19.17	17.58	0.1972	Early	none	
301646	12 16 49.06	−0 44 31.2	0.78	12.07	16.08	14.99	0.0709	Early	none	
301882	12 14 6.72	+0 26 34.5	0.85	2.27	18.62	17.36	0.1837	Early	none	
302322	12 25 26.79	−2 31 25.0	1.10	1.97	19.25	18.09	0.1988	Early/E+AGN	O III	
302370	12 24 22.56	−2 11 7.6	0.68	2.21	17.34	17.53	0.0855	Late	Hα,Hβ,O II,O III,S II	
302382	12 23 57.35	−2 33 14.0	0.45	1.97	18.90	17.85	0.1987	Sy2	O III,Hα,N II,O II,Hβ	O:Interaction
302412	12 22 53.52	−1 39 28.3	1.24	2.99	18.89	?	0.1871	Early	none	
302433	12 22 36.05	−2 23 12.5	0.53	1.17	18.42	18.00	0.1319	Early	Hα	
302518	12 20 52.06	−2 9 23.8	0.37	2.52	17.17	16.64	0.0675	Early	none	
302576	12 19 27.87	−1 38 24.1	1.68	1.00	19.04	18.12	0.1441	Early	Hα,N II,O II,O III	
302579	12 19 20.86	−2 0 26.9	0.38	6.31	18.05	18.02	0.1308	E+AGN	Hα,N II,O II,O III,Hβ	
302819	12 14 12.07	−2 4 40.4	0.46	1.98	18.79	17.71	0.1591	Early	none	
302830	12 13 54.49	−1 44 25.0	0.44	1.34	18.50	18.13	0.1627	E+AGN	O III,Hα,N II,O II,Hβ	
302889	12 12 48.24	−2 43 29.5	0.34	2.91	15.51	13.84	0.0387	Late	Hα,N II,S II,Hβ,O III,O II	
303266	12 45 28.86	+0 58 30.4	0.12	4.54	17.43	17.27	0.0820	Early	none	
303750	12 39 4.23	+0 58 15.6	0.16	5.57	17.12	16.90	0.0731	Early	none	
304197	12 51 56.38	−0 35 48.3	0.66	1.73	16.66	16.39	0.0835	Early	Hα,O II	
304271	12 50 59.10	−0 25 21.7	0.82	2.81	18.68	?	0.1912	Early	none	

Table 2 – *continued*

Object	α (J2000)	δ (J2000)	Off	S1.4	bJ	R	z	Class	Emission Lines	Notes
304283	12 50 42.44	+0 19 57.0	0.22	1.64	19.02	17.84	0.1254	E+AGN	N II,Hα,O III,S II,O II	
304312	12 50 21.52	+0 12 42.8	0.92	2.76	17.94	18.22	0.0812	Early	Hα	
304375	12 49 33.62	−0 45 53.0	0.38	1.00	19.45	?	0.1940	Early	none	
304423	12 48 50.36	+0 29 48.3	0.38	6.07	18.08	17.76	0.1072	Early	none	
304723	12 46 34.50	+0 7 43.3	0.76	3.19	17.93	18.08	0.0715	Early	none	
304763	12 46 17.51	−0 16 58.3	0.11	1.06	18.24	17.86	0.1265	Early	none	
304783	12 46 5.76	+0 18 45.5	1.61	1.43	17.31	18.17	0.0832	Late	Hα,N II,Hβ,O III,O II	O:Spiral
304900	12 44 52.09	−1 4 45.3	0.36	2.13	18.97	18.69	0.1257	Early	O II	
305063	12 43 21.75	+0 15 36.4	0.55	1.87	19.23	18.48	0.1429	Sy2	O III,Hα,N II,O II,S II	
305075	12 43 9.64	+0 30 33.1	0.16	2.50	17.56	18.17	0.0905	Late	Hα,S II,O II	
305185	12 42 12.98	−0 5 54.9	1.99	1.12	16.51	14.90	0.0471	Early	none	
305276	12 40 54.57	−1 7 22.3	1.31	1.02	19.19	18.29	−.0005	Star	none	
305349	12 39 41.14	−1 13 35.0	0.20	2.37	19.30	18.08	0.1877	Early	none	
305401	12 39 1.08	+0 21 56.9	1.36	2.06	15.39	13.70	0.0229	Early	none	
305470	12 38 6.19	−0 42 15.3	0.28	1.29	19.06	18.40	0.0913	Early	Hα	
305472	12 38 3.36	+0 4 55.4	1.35	1.16	18.15	18.58	0.1166	Late	Hα,N II,O II,S II,Hβ	
305508	12 37 43.67	−0 16 11.4	1.35	1.01	18.28	17.82	0.1084	Early	none	
305590	12 36 35.93	−0 32 53.6	0.91	1.42	19.30	18.15	0.2326	Early	O II	
305607	12 36 22.97	−0 52 4.3	0.47	9.18	18.74	17.91	0.1423	Early	none	
305657	12 35 40.70	−0 34 59.4	1.14	1.22	19.19	17.84	0.2327	Early	O II	
305788	12 33 36.39	−0 56 48.4	0.52	1.56	18.26	?	0.1118	Late	Hα,N II,S II,Hβ	O:Interaction
305966	12 51 29.71	−1 50 19.2	0.51	1.52	17.34	14.74	0.0820	Early	none	
306761	12 43 27.38	−1 50 49.5	0.84	2.76	18.09	18.31	0.0809	Early	Hα,N II,O II	
306862	12 42 12.62	−2 8 51.3	1.57	5.18	15.77	14.47	0.0833	Early	none	
306984	12 40 26.75	−2 7 10.1	1.08	1.09	17.81	18.46	0.0882	Late	Hα,Hβ,S II,O II,O III	
307070	12 38 50.21	−2 29 37.3	1.58	2.95	18.24	17.44	0.1373	Early	Hα,N II	O:Merging
307098	12 38 24.60	−1 33 41.2	1.03	1.94	18.59	18.65	0.1880	Late	Hα,N II,O II,Hβ,O III	O:Irregular
307156	12 37 51.48	−1 18 13.4	0.21	3.86	18.65	17.55	0.1537	Early	none	
307163	12 37 45.89	−1 14 16.0	1.01	7.57	17.37	16.86	0.1353	Early	none	
307226	12 37 6.76	−2 6 10.2	1.87	7.63	17.56	17.29	0.1114	Early	O II	O:Interaction
307364	12 34 27.80	−1 41 1.1	0.60	1.67	19.44	18.70	0.3179	Late	O II,Hβ,O III	
307556	13 12 20.95	+0 7 1.3	0.23	5.87	19.22	17.16	0.2125	Late	Hβ	
307671	13 11 56.94	+0 13 51.1	0.63	92.15	19.04	16.37	0.2119	Early	none	R:Double
307794	13 11 32.12	−0 37 16.5	0.99	3.24	16.97	15.99	0.0403	Late	Hα,S II,Hβ,O II	
308664	13 8 18.51	−1 16 9.0	0.78	1.85	18.60	16.99	0.0847	E+AGN	Hα,N II,O III,O II	
309027	13 6 32.99	+0 22 49.0	1.47	7.90	18.46	17.06	0.1476	E+AGN	Hα,N II,S II,O III,O II	O:Interaction
309125	13 6 2.03	+0 14 50.7	1.87	1.94	18.96	17.08	0.1731	Early	none	
309130	13 6 1.48	+0 1 26.1	0.73	1.78	18.83	17.90	0.1377	Late	Hα,O III,Hβ,O II,S II	
309173	13 5 51.44	−1 19 4.6	0.10	1.88	17.84	17.33	0.0964	Late	Hα,O II,O III,S II,Hβ	
309188	13 5 47.66	−0 23 9.7	0.26	1.89	17.29	16.17	0.0314	Late	Hα,S II,Hβ,O II,O III	
309335	13 5 7.10	−0 9 44.0	0.40	1.47	18.19	17.39	0.1242	Late	Hα,O II,Hβ,O III,S II	
309408	13 4 44.39	−0 15 35.0	0.32	2.63	18.33	17.62	0.1974	Late	Hα,O III,Hβ,O II	
309643	13 3 26.53	+0 13 27.2	0.43	3.39	18.71	16.90	0.2084	Early	none	
309726	13 3 0.28	−0 28 53.3	0.21	3.35	17.87	16.18	0.0828	Early	none	
310170	13 1 5.58	+0 45 31.1	1.39	3.78	16.31	14.09	0.0820	Early	none	
310333	13 0 23.22	−0 3 9.9	0.87	1.38	19.04	18.07	0.0818	Late	Hα,Hβ,O II,O III,S II	
310901	12 55 9.62	+0 58 16.4	0.92	1.58	18.69	?	0.1327	Early	none	
311215	12 55 54.58	−0 59 56.8	0.72	1.59	16.76	15.51	0.0475	Early	none	
311234	12 55 49.16	−1 38 39.6	0.74	1.76	19.32	?	0.2366	Early	none	
311323	12 55 16.55	+0 14 48.7	0.32	2.31	15.57	14.58	0.0477	Early	none	
311411	12 54 52.68	−0 30 9.1	0.56	4.50	18.54	17.89	0.1266	E+AGN	O III,Hα,N II,S II,O II	
311811	12 53 5.21	+0 15 55.9	0.58	1.30	17.87	17.73	0.0710	E+AGN	O III,Hα,N II,O II,Hβ,S II	
311992	13 31 52.85	+2 1 0.6	1.46	11.25	17.31	17.09	0.0863	E+AGN	Hα,N II,O III,S II	
312170	13 30 7.02	+0 31 54.7	0.83	2.80	17.19	?	0.0757	Late	Hα,Hβ,O III,O II	
312259	13 29 2.38	+1 54 1.3	0.09	1.12	18.24	17.71	0.1123	Early	none	
312273	13 28 53.33	+2 0 20.6	1.42	2.01	19.24	?	0.1402	Early	N II,O III	
312292	13 28 41.88	+2 1 40.7	0.27	10.24	18.15	16.44	0.1398	Early	none	
312296	13 28 38.99	+0 32 54.6	0.37	5.06	17.75	16.69	0.1046	Early	O II	
312466	13 26 55.80	+0 41 53.8	1.31	3.84	17.49	17.70	0.0822	E+AGN	O III,Hα,N II,O II,S II,Hβ	O:Irregular
312604	13 25 6.35	+1 51 45.5	0.74	2.85	17.72	17.65	0.0582	Late	Hα,S II,O II	
312660	13 24 35.99	+1 36 30.5	1.33	2.14	18.18	19.17	0.1067	Late	Hα,O III,O II,Hβ,S II	
312686	13 24 25.64	+0 37 45.6	0.28	1.34	19.13	17.32	0.2163	Early	none	
312805	13 23 21.55	+1 56 31.8	1.26	3.28	17.32	17.34	0.1100	Late	Hα,S II,O II,Hβ	
312875	13 22 30.22	+0 53 28.3	1.26	1.92	19.01	17.75	0.1840	Early	O II	
312939	13 21 23.33	+1 23 30.1	0.12	1.05	18.06	18.12	0.1356	Late	Hα,O III,Hβ,O II	
312972	13 21 0.51	+1 16 9.8	0.50	11.08	18.27	17.51	0.1480	Early	Hα,O II	
313111	13 19 44.09	+1 48 18.8	1.78	1.23	19.05	?	0.2237	Early	none	
313143	13 19 15.04	+1 39 17.3	1.46	3.47	18.54	17.45	0.1414	Early	none	
313278	13 17 31.98	+1 51 28.2	0.98	5.58	17.15	16.09	0.0785	Early	none	
314024	13 27 39.53	+0 19 18.0	0.72	4.35	16.87	16.80	0.0468	Late	Hα,S II,Hβ,O III,O II	
314123	13 26 32.24	+0 28 1.3	0.46	1.15	18.58	18.31	0.0852	Late	Hα,Hβ,S II,O III,O II	

Table 2 – *continued*

Object	α (J2000)	δ (J2000)	Off	S1.4	bJ	R	z	Class	Emission Lines	Notes
314131	13 26 25.77	− 0 21 48.5	0.04	1.11	19.08	18.40	0.1906	Early	O II	
314229	13 25 34.50	+ 0 15 22.4	0.69	5.97	18.58	17.34	0.1761	E+AGN	O III	
314389	13 23 56.90	+ 0 10 50.6	0.39	10.66	19.00	?	0.2270	Early	none	
314683	13 21 23.13	+ 0 20 32.7	1.05	33.00	14.46	?	0.0181	Late	Hα,S II,O III	O:Spiral
314685	13 21 23.26	+ 0 4 41.9	0.52	2.02	17.34	17.57	0.0848	E+AGN	Hα,N II,O III,S II,Hβ	
317526	13 48 6.39	+ 0 49 20.1	1.45	1.82	17.47	17.46	0.0886	Early	none	
318360	13 34 25.73	+ 0 56 46.9	0.92	5.75	19.28	?	0.2476	Early	none	R:Core+lobes
318462	13 32 51.75	+ 0 48 49.2	0.21	1.93	19.18	18.32	0.1721	Late	Hα,Hβ,O II,O III,S II	
318617	13 50 2.07	+ 0 1 51.1	0.75	1.67	18.83	18.12	0.2031	Late	Hα,Hβ,O II,O III	
318618	13 50 4.77	− 0 8 52.3	0.89	1.96	18.82	18.30	0.1015	Late	Hα,Hβ,S II,O III,O II	
318703	13 48 35.47	− 0 57 46.9	0.75	7.58	18.71	17.53	0.1657	Early	none	
318766	13 47 28.39	− 0 53 46.9	0.54	4.44	17.95	17.65	0.0763	Early	none	
318837	13 46 21.77	− 0 52 29.0	0.76	8.53	17.02	17.75	0.0766	SB	Hα,N II,Hβ,S II,O II,O III	
318838	13 46 23.23	− 0 52 37.4	0.89	1.25	17.47	18.05	0.0769	Late	Hα,N II,Hβ,S II,O II	
318871	13 46 7.09	− 0 16 56.6	1.95	1.36	18.35	17.26	0.2155	Early	none	
318894	13 45 52.84	− 0 46 7.6	0.85	21.41	17.93	17.39	0.1486	Early	none	
319035	13 44 28.36	+ 0 1 46.5	0.93	8.01	18.34	17.35	0.1351	Early	none	
319207	13 42 12.20	− 0 17 38.1	0.19	1.50	18.17	18.00	0.0866	E+AGN	N II,S II	
319235	13 41 59.43	− 0 34 46.4	0.59	1.69	17.69	17.66	0.0869	Early	none	
319470	13 39 2.30	+ 0 29 12.9	0.71	1.73	18.78	17.70	0.1437	Early	none	
319508	13 38 30.69	− 0 42 6.2	0.72	1.97	18.12	17.79	0.0719	Late	Hα,N II,Hβ,O II,O III,S II	

Table 3. As in Table 2.

Object	α (J2000)	δ (J2000)	Off	S1.4	bJ	R	z	Class	Emission Lines	Notes
319681	13 35 38.77	− 0 55 12.8	0.52	3.77	16.29	17.04	0.0721	Late	Hα,N II,Hβ,S II	
319838	13 32 54.58	− 0 32 35.7	1.01	1.03	17.64	17.18	0.0871	Late	Hα,N II,Hβ,O III,O II,S II	
320158	13 46 16.50	− 2 27 41.8	1.05	1.39	18.89	17.39	0.2188	Early	none	R:Double
320199	13 45 29.89	− 1 40 2.8	0.99	3.98	18.08	17.84	0.0877	Late	Hα,S II,O II	
320216	13 45 16.85	− 1 56 25.9	0.53	374.6	17.98	?	0.1498	Early	O II	
320257	13 44 44.07	− 2 24 8.0	1.25	34.51	18.83	?	0.0848	Early	none	O:Irregular R:Extended
320321	13 42 57.58	− 1 56 41.2	0.74	1.55	17.50	18.18	0.0889	Late	Hα,Hβ,S II,O II	
320332	13 42 38.39	− 1 33 17.8	0.73	3.76	17.72	17.57	0.0272	Late	Hα,N II,S II,O III	
320517	13 39 17.32	− 1 50 49.3	0.55	57.47	17.08	17.64	0.0891	Early	none	R:Double
320550	13 38 49.45	− 2 22 37.4	0.76	11.55	18.92	17.78	0.2191	Early	O II	
320595	13 38 1.50	− 1 47 11.3	0.50	3.58	18.76	17.48	0.1774	Eary	none	
320603	13 37 54.33	− 2 2 56.0	1.08	3.50	17.28	17.15	0.0897	Early	none	
320613	13 37 44.06	− 2 10 27.8	1.12	4.96	16.78	17.33	0.0265	SB	Hα,N II,S II,Hβ,O II,O III	
320922	14 12 23.46	− 0 49 29.4	0.23	14.88	19.11	17.40	0.1877	Early	none	
320956	14 12 15.42	− 1 8 1.1	0.64	1.12	19.37	17.28	0.1810	Early	none	
320957	14 12 15.56	− 0 38 0.4	1.13	8.35	15.53	15.75	0.0258	Late	Hα,N II,S II	
321035	14 11 54.09	− 0 48 0.4	1.09	1.63	17.44	18.61	0.0978	Late	Hα,N II,S II,Hβ,O II	
321986	14 8 12.30	− 2 24 9.2	0.36	1.60	18.30	17.80	0.1285	Late	Hα,N II,Hβ,O III,O II,S II	
322005	14 8 8.50	− 1 42 9.2	1.88	2.29	14.10	12.70	0.0250	Late	Hα,N II	O:Spiral
322020	14 8 3.14	+ 0 2 57.3	1.36	2.27	17.60	18.94	0.0851	Late	Hα,Hβ,O II,O III,S II	
322636	14 5 13.75	− 1 14 56.8	1.58	1.72	15.61	15.51	− .0002	Star	none	
322760	14 4 33.84	+ 0 12 14.0	1.09	2.04	19.42	18.04	0.2557	Sy2	O III,O II,Hβ	
322822	14 4 17.65	− 1 27 40.7	0.99	1.42	18.50	17.88	0.1159	Late	Hα,N II,S II,O II,Hβ	
322925	14 3 50.92	− 0 31 13.9	0.90	3.56	19.33	17.55	0.1843	Early	none	
322958	14 3 42.42	− 0 51 3.6	0.64	1.45	18.14	18.61	0.0939	Late	Hα,N II,S II,O II,Hβ	
323057	14 3 8.82	+ 0 24 46.2	1.22	7.71	18.82	16.25	0.1822	Early	none	R:Double
323317	14 1 41.72	+ 0 45 56.5	0.83	1.62	18.74	17.60	0.1668	Early	none	
323342	14 1 38.67	− 1 38 44.5	1.39	1.17	17.93	17.89	0.1043	Early	Hα,N II,O II	
323346	14 1 38.21	− 2 30 23.6	0.55	4.66	19.24	17.51	0.2172	E+AGN	O III	
323400	14 1 18.98	− 2 11 26.9	0.19	3.86	17.91	?	0.1717	E+AGN	Hα,N II,O III,Hβ,O II	
323429	14 1 7.32	− 1 43 40.7	0.57	2.21	18.38	17.41	0.1454	Early	Hα	
323518	14 0 40.53	− 1 55 18.5	1.12	2.69	17.04	17.25	0.0250	Sy2	Hα,N II,O III,Hβ,O II	
323604	14 0 16.23	− 1 32 8.7	0.55	1.77	19.14	17.73	0.1463	E+AGN	Hα,N II,O III,S II,O II	
323803	13 59 30.17	− 2 27 2.8	0.27	3.58	19.35	17.16	0.2231	Early	none	
323838	13 59 18.05	− 0 57 27.7	1.70	1.19	18.49	17.90	0.1063	E+AGN	Hα,N II,S II,O III	
323970	13 58 42.25	− 0 17 34.5	0.24	1.66	19.31	17.67	0.1886	Early	none	
323971	13 58 42.03	− 0 39 29.5	0.35	13.11	17.57	16.54	0.1314	Early	none	
324016	13 58 25.23	+ 0 58 58.0	0.42	56.04	18.06	17.85	0.1379	E+AGN	N II,O III,O II	
324044	13 58 20.01	− 2 21 41.9	0.77	1.79	19.35	17.19	0.2200	Early	none	
324175	13 57 42.60	− 1 37 36.0	0.22	1.41	18.71	17.11	0.1462	Early	O II	
324361	13 56 45.17	− 0 8 52.5	0.50	2.84	17.09	18.36	0.1074	Late	Hα,N II,Hβ,S II,O II	
324410	13 56 27.29	− 0 17 17.6	1.07	13.08	15.26	?	0.0295	Early	Hα,N II,O II	O:Irregular
324444	13 56 17.76	− 2 31 2.1	0.16	1.84	18.71	17.66	0.1348	Sy2	O III,Hα,N II,Hβ,O II	

Table 3 – *continued*

Object	α (J2000)	δ (J2000)	Off	S1.4	bJ	R	z	Class	Emission Lines	Notes
324480	13 56 6.37	− 0 9 30.7	0.41	2.54	19.32	0.00	0.1960	Early	none	
324533	13 55 47.66	+0 48 45.5	0.62	2.40	17.59	18.16	0.0863	Late	Hα,N II,Hβ,S II,O II,O III	
324932	13 53 26.22	+0 2 48.0	0.47	3.07	17.39	?	0.1162	Early	O II	
325067	13 52 51.65	− 2 36 32.9	1.89	12.81	16.15	16.15	0.0756	Early	O II	
325549	14 25 53.61	+0 34 49.2	0.92	2.14	17.39	16.88	0.1284	Early	none	
325666	14 23 26.77	+0 57 18.0	1.14	4.03	17.98	17.66	0.1260	Early	none	
326267	14 14 17.54	+0 40 17.3	1.11	3.04	17.79	16.71	0.1140	Early	none	
326469	14 31 8.65	− 0 25 30.7	0.38	2.26	18.46	18.72	0.0925	Late	Hα,S II,Hβ,O II,O III	
326530	14 30 26.20	− 1 7 54.2	1.60	2.61	18.02	?	0.1229	Early	none	
326677	14 28 16.50	+0 0 8.6	0.49	1.72	18.38	18.78	0.0529	Late	Hα,S II,Hβ,O III,O II	
326693	14 27 55.12	− 0 33 44.5	0.40	2.36	17.05	16.91	0.0786	Late	Hα,N II,O II	
326755	14 26 46.89	− 0 30 33.7	1.54	1.27	19.06	18.66	0.2530	Late	Hβ,O III,O II	
326795	14 25 55.09	− 0 16 17.5	0.32	1.39	18.49	18.54	0.1293	E+ AGN	Hα,N II,O III,O II,Hβ	
326865	14 25 7.41	− 1 2 50.5	1.48	2.91	17.97	18.00	0.1038	Early	Hα	
326877	14 24 52.12	+0 8 20.7	0.73	5.53	18.89	18.80	0.1311	Sy2	O III,Hα,N II,O II,Hβ	
326886	14 24 44.96	− 0 19 30.5	0.53	13.95	18.54	17.46	0.1737	Early	none	
326931	14 24 3.40	+0 29 57.8	1.00	74.40	17.54	16.98	0.1247	Early	none	R:Core+Jets
327076	14 21 56.60	− 0 42 3.8	1.03	1.52	18.20	18.70	0.0532	Early	Hα	
327106	14 21 31.00	− 0 12 47.5	0.82	1.98	17.77	18.16	0.0516	E+ AGN	N II	
327121	14 21 10.91	− 0 47 13.5	1.12	1.96	18.59	18.38	0.1269	E+ AGN	N II	
327124	14 21 7.33	− 1 7 26.4	0.70	2.24	19.06	18.83	0.1296	Late	Hα,N II,S II,O II,O III,Hβ	
327253	14 18 35.13	− 0 40 58.3	1.34	1.52	17.94	?	0.1507	Early	N II,O II	O:Merging
327261	14 18 31.65	− 0 51 25.4	1.03	2.09	17.00	16.48	0.0503	Early	O II	
327345	14 17 27.57	− 0 25 36.5	0.50	2.81	18.67	18.33	0.1226	Late	Hα,N II,Hβ,S II,O II	
327497	14 15 38.95	− 0 27 40.7	1.02	2.61	17.95	17.07	0.0833	Early	none	
327499	14 15 41.24	− 0 38 52.4	1.01	1.93	18.84	17.42	0.1482	Early	O II	
327534	14 15 16.23	+0 28 38.5	0.06	1.62	18.49	17.50	0.1440	Early	none	
327586	14 14 57.72	− 0 20 58.9	0.25	3.71	18.06	16.79	0.1388	Early	O II	
327597	14 14 52.55	+0 11 45.9	0.44	1.81	17.81	16.67	0.1239	Early	none	
327624	14 14 43.60	− 0 16 56.3	1.60	2.36	16.04	15.63	0.0382	SB	Hα,N II,S II,Hβ	
327653	14 14 31.05	− 0 30 43.5	0.41	2.24	18.87	17.98	0.1375	Late	Hα,N II,Hβ,O II	
327679	14 14 16.26	− 0 21 4.9	0.23	2.82	18.97	18.00	0.1392	Early	none	
327730	14 13 51.80	− 0 37 51.0	1.00	7.83	18.70	?	0.1212	Early	none	
327732	14 13 49.10	− 0 46 31.3	0.76	1.82	17.41	16.95	0.1196	Early	none	
327862	14 32 9.60	− 2 11 36.4	0.43	46.30	18.07	17.22	0.1227	Early	none	
327910	14 31 16.21	− 1 42 35.1	1.18	14.14	18.94	17.31	0.2208	Early	none	
328104	14 27 29.67	− 2 5 33.8	0.56	6.44	18.12	18.27	0.0545	Late	Hα,N II,S II,O II	
328129	14 27 6.79	− 2 13 26.5	0.52	1.99	18.34	?	0.0816	Late	Hα,N II,Hβ	
328517	14 18 21.99	− 2 35 57.7	1.67	1.56	18.80	17.23	0.1847	Early	none	
328529	14 18 8.82	− 1 22 34.8	0.70	22.09	19.11	17.91	0.1530	Early	none	R:Core+Jets
328672	14 15 17.98	− 2 26 42.1	0.93	18.88	15.47	14.24	0.0469	Early	N II	O:Bulge+Disk
328739	14 14 17.71	− 2 31 4.3	0.60	3.28	16.87	16.49	0.0758	Sy2	O III,Hα,N II,S II,O II,Hβ	
328764	14 13 45.46	− 1 52 54.7	0.57	1.27	18.17	18.01	0.1199	Late	Hα,N II,S II,Hβ,O II,O III	
328909	14 51 3.12	+0 40 58.7	1.58	2.81	17.35	16.86	0.0690	Late?	Hα	
328986	14 49 37.81	+0 50 34.0	0.99	6.95	19.14	?	0.2116	Early	none	
329113	14 47 26.30	+0 50 16.3	0.25	2.35	18.47	16.28	0.1716	Early	none	
329976	14 33 35.30	+0 54 26.5	1.69	1.30	17.77	15.86	0.1196	Early	none	
330250	14 50 19.21	− 1 6 47.4	0.83	96.34	18.27	16.94	0.1197	Sy2	O III,Hα,N II,S II,O II,Hβ	R:Double
330312	14 49 28.63	− 1 16 17.6	1.78	40.16	18.38	?	0.2020	Early	none	R:Extended
330372	14 48 27.54	− 0 6 45.0	1.12	4.41	19.25	18.03	0.1379	Early	Hα	
330921	14 40 13.79	+0 0 38.9	0.66	12.21	18.62	15.89	0.1790	Early	none	R:Double
331094	14 38 6.75	+0 32 20.3	0.31	2.30	19.14	18.05	0.2095	E+ AGN	O III,Hα,N II,O II,Hβ	
331135	14 37 43.73	− 0 18 56.0	1.90	3.94	17.42	15.17	0.1379	Early	none	
331138	14 37 43.35	− 0 27 45.9	0.84	2.30	18.55	16.57	0.1407	Early	none	
331148	14 37 41.75	− 0 55 15.7	0.70	3.48	18.56	16.88	0.1481	Early	O II	
331172	14 37 27.78	− 0 23 43.6	0.77	10.08	19.12	17.59	0.1377	E+ AGN	Hα,N II,O III,O II	
331437	14 34 52.70	− 0 28 28.1	0.44	42.27	19.33	?	2.2485	Sy1	C III,C IV,Lyα	
331441	14 34 54.37	− 1 16 18.2	1.24	1.61	17.53	?	0.0560	Late	Hα,S II,O III,O II	
331488	14 34 15.35	− 0 58 9.2	0.62	11.99	19.00	16.74	0.2188	Early	none	
331921	14 47 7.52	− 2 8 45.4	0.12	2.79	18.02	17.23	0.0710	Late	Hα,N II,S II,Hβ,O III,O II	
332005	14 45 31.14	− 1 35 18.8	0.83	1.88	18.96	16.82	0.1494	Early	none	
332224	14 40 44.25	− 2 36 24.0	1.19	1.59	17.84	16.96	0.1047	Late	Hα,N II,S II,Hβ,O II	
332351	14 38 46.68	− 1 30 5.1	0.54	3.75	19.26	17.33	0.1395	Early	O II	
332426	14 37 40.75	− 2 22 14.3	0.95	2.38	19.01	?	0.1204	Late	Hα,N II,S II,Hβ,O II	
332642	14 33 40.95	− 1 45 3.5	0.16	2.73	18.79	16.32	0.2194	Early	none	O:Interaction
332679	14 32 45.57	− 1 35 51.4	0.43	1.94	18.99	18.08	0.2210	Early	none	

and $z = 0.2$, mainly classical AGN-fuelled galaxies. Above $z = 0.2$ the optical apparent magnitude limit means the sample loses the fainter galaxies.

Fig. 11 shows that the contribution of actively star-forming galaxies (spirals and irregulars) to the local radio population is less important than previously thought (see, e.g., Dunlop & Peacock 1990, where the distributions in redshift derived from their seven models for sources with $S \geq 1$ mJy show remarkable 'spikes' for $z \lesssim 0.05$, as shown by Magliocchetti et al. 2000). Our findings, however, agree with the results from Jackson & Wall (1999), who claim ~ 30 per cent of the sources at 1 mJy to be starburst/ starforming galaxies. As the analysis performed in Sections 3 and 4 indicates, these sources are then most likely to be identified with the radio counterparts of the dusty/starforming *IRAS* galaxies.

Unfortunately, the question of whether star-forming objects are strongly evolving with redshift (as claimed by, for instance, Rowan-Robinson et al. 1993) or not (see, e.g., Dunlop & Peacock 1990) has to be left unanswered, since the limited redshift range of the spectroscopic sample does not allow any evolutionary analysis. We note, however, that the fact that late-type galaxies in the spectroscopic sample are in general found quite locally seems to argue against positive luminosity evolution, which would make these sources brighter at higher redshifts, and therefore observable by a $S \geq 1$ mJy-limited radio survey such as FIRST beyond $z \sim 0.1$.

6 CONCLUSIONS

In this work we have used data from the 2dF Galaxy Redshift Survey to derive the properties of local $S \geq 1$ mJy radio sources. The radio sample was drawn from the FIRST catalogue and all the objects lie within the area $9^{\mathrm{h}}48^{\mathrm{m}} \lesssim \mathrm{RA}(2000) \lesssim 14^{\mathrm{h}}32^{\mathrm{m}}$ and $-2°.77 \lesssim \mathrm{Dec.}(2000) \lesssim 2°.25$, where the FIRST and APM surveys overlap. 971 radio sources were found to have optical counterparts brighter than $b_J = 19.45$ in the APM Galaxy catalogue; the 2dFGRS has then provided spectra and redshift measurements for 557 of them (the spectroscopic sample), up to $z \simeq 0.3$. We note that this apparent incompleteness is merely due to incomplete sky coverage of the spectroscopic survey, since neither radio nor magnitude biases have been found in the determination of both the optical and spectroscopic counterparts of FIRST radio sources.

Sources in the spectroscopic sample have been divided into three broad classes on the basis of their spectral appearance.

(1) 'Classical' radio galaxies (i.e., sources with a spectrum typical of absorption systems plus the eventual presence of emission lines due to AGN activity): 350 objects corresponding to 63 per cent of the sample, appearing for $z \gtrsim 0.1$ and showing relative high radio-to-optical ratios, red colours and radio powers $10^{21} \lesssim P_{1.4\,\mathrm{GHz}}/\mathrm{W\,Hz}^{-1}\,\mathrm{sr}^{-1} \lesssim 10^{24}$. These objects – likely to be classical FRI sources – also present absolute magnitudes distributed within a narrow interval around $M_B \simeq -21.3$, a result which highlights their 'standard-candle' nature.

(2) Late-type galaxies and starbursts: 177 objects, corresponding to about 32 per cent of the spectroscopic sample, mainly present in the very nearby Universe ($z \lesssim 0.1$), showing blue colours, faint radio luminosities ($P_{1.4\,\mathrm{GHz}} \lesssim 10^{21.5}\,\mathrm{W\,Hz}^{-1}\,\mathrm{sr}^{-1}$) and low radio-to-optical ratios ($r \lesssim 10^3$).

(3) Seyfert galaxies: 18 Seyfert 2 and four Seyfert 1 (one at $z = 2.24$) galaxies are included in the spectroscopic sample.

When available, radio and optical images have also allowed morphological studies of the sources in the sample. As an

interesting result, we find that the majority of the radio sources observed by the 2dFGRS as merging/interacting systems, present spectra typical of early-type galaxies, suggesting that, under appropriate conditions, galaxy–galaxy interaction can trigger AGN activity even at low redshifts.

Analysis of the local radio luminosity function for the spectroscopic sample shows that, for $P_{1.4\,\mathrm{GHz}} \gtrsim 10^{20.5}\,\mathrm{W}$ $\mathrm{Hz}^{-1}\,\mathrm{sr}^{-1}$, classical radio galaxies are well described by models such as the one introduced by Dunlop & Peacock (1990) for pure luminosity evolution, although we note that no estimate of the evolutionary degree of this population was possible due to the limited redshift range spanned by the 2dFGRS.

Late-type galaxies instead exhibit a broken power-law trend for their luminosity function. Such a break and the rapid decrease of the number density of sources for $P_{1.4\,\mathrm{GHz}} \gtrsim 10^{22}\,\mathrm{W\,Hz}^{-1}\,\mathrm{sr}^{-1}$ explains the quick disappearance of this class of objects beyond $z \simeq 0.1$ as shown by their redshift distribution. The observed LF in this case is in agreement with the one derived by Saunders et al. (1990) for *IRAS* galaxies. This supports the assumption of Rowan-Robinson et al. (1993) that late-type radio galaxies should be identified with the population of dusty spirals and starbursts observed at 60 μm.

REFERENCES

Becker R. H., White R. L., Helfand D. J., 1995, ApJ, 450, 559
Benn C. R., Rowan-Robinson M., McMahon R. G., Broadhurst T. J., Lawrence A., 1993, MNRAS, 263, 98
Blandford R. D., Rees M. J., 1974, MNRAS, 169, 395
Bock D. C-J., Large M. I., Sadler E. M., 1999, AJ, 117, 1578
Colless M. et al. (2dFGRS team), 2001, MNRAS, 328, 1039
Condon J. J., 1984, ApJ, 287, 461
Condon J. J., Cotton W. D., Greisen E. W., Yin Q. F., Perley R. A., Taylor G. B., Broderick J. J., 1998, AJ, 115, 1693
Danese L., De Zotti G., Franceschini A., Toffolatti L., 1987, ApJ, 318, L15
Dunlop J. S., Peacock J. A., 1990, MNRAS, 247, 19
Fanaroff B. L., Riley J. M., 1974, MNRAS, 167, L31
Folkes S. R. et al., 1999, MNRAS, 308, 459
Georgakakis A., Mobasher B., Cram L., Hopkins A., Lidman C., Rowan-Robinson M., 1999, MNRAS, 306, 708
Gruppioni C., Mignoli M., Zamorani G., 1999, MNRAS, 304, 199
Hill T. L., Heisler C. A., Norris R. P., Reynolds J. E., Hunstead R. W., 2001, ApJ, 548, 127
Jackson C. A., Wall J. V., 1999, MNRAS, 304, 160
Kennicutt R. C., 1992, ApJ, 388, 310
Kochanek C. S., Pahre M. A., Falco E. E., 2002, ApJ, submitted (astro-ph/0011458)
Ledlow M. J., Owen F. N., 1996, AJ, 112, 9
Maddox S. J., 1998, in D'Odorico S., Fontana A., Giallongo E., eds, Large-Scale Structure: Tracks and Traces, proc. 12th Postdam Cosmogony Workshop. World Scientific, p. 91
Maddox S. J., Efstathiou G., Sutherland W. J., Loveday J., 1990a, MNRAS, 243, 692
Maddox S. J., Efstathiou G., Sutherland W. J., 1990b, MNRAS, 246, 433
Maddox S. J., Efstathiou G., Sutherland W. J., 1996, MNRAS, 283, 1227
Madgwick D. et al. (2dFGRS team), 2002, MNRAS, submitted (astro-ph/0107197)
Magliocchetti M., Maddox S. J., 2002, MNRAS, 330, 241
Magliocchetti M., Maddox S. J., Lahav O., Wall J. V., 1998, MNRAS, 300, 257
Magliocchetti M., Maddox S., Wall J. V., Benn C. R., Cotter G., 2000, MNRAS, 318, 1047
Maraschi L., Rovetti F., 1994, ApJ, 436, 79
Masci F. J. et al., 2001, PASP, 113, 10
McQuade K., Calzetti D., Kinney A. L., 1995, ApJS, 97, 331

Oort M. J. A., Steemers W. J. G., Windhorst R. A., 1988, A&AS, 73, 103

Orr M. J. L., Browne I. W. A., 1982, MNRAS, 200, 1067

Padovani P., Urry C. M., 1992, ApJ, 387, 449

Rixon G. T., Wall J. V., Benn C. R., 1991, MNRAS, 251, 243

Rola C., Terlevich E., Terlevich R., 1997, MNRAS, 289, 419

Rowan-Robinson M., 1968, MNRAS, 138, 445

Rowan-Robinson M., Benn C. R., Lawrence A., McMahon R. G., Broadhurst T. J., 1993, MNRAS, 263, 123

Sadler E. M., McIntyre V. J., Jackson C. A., Cannon R. D., 1999, Proc. Astron. Soc. Aust., 16, 247

Sadler E. M. et al. (2dFGRS team), 2002, MNRAS, 329, 227

Saunders W., Rowan-Robinson M., Lawrence A., Efstathiou G., Kaiser N., Ellis R. S., Frenck C. S., 1990, MNRAS, 242, 318

Veilleux S., Osterbrock D. E., 1987, ApJS, 63, 295

Wall J. V., Jackson C. A., 1997, MNRAS, 290, L17

Wall J. V., Pearson T. J., Longair M. S., 1980, MNRAS, 193, 686

Windhorst R. A., Miley G. K., Owen F. N., Kron R. G., Koo R. C., 1985, ApJ, 289, 494

Woltjer L., 1990, in Blandford R., Netzer H., Woltjer L., eds, SAAS-FEE Advanced Course on Active Galactic Nuclei, Swiss Society for Astro-Physics Astronomy

This paper has been typeset from a TEX/LATEX file prepared by the author.